MATHEMATICAL MODELING OF PROPELLER WAKE WASH FOR PACK-ICE MANAGEMENT

by

© Tony Bastin

A thesis submitted to the School of Graduate Studies

in partial fulfillment of the requirements for the degree of

Master's of Engineering

Ocean Engineering and Naval Architecture

Memorial University of Newfoundland

May 2015

St. John’s, Newfoundland

ABSTRACT

Propeller wake wash has been used effectively for ice management operations for years. The main uses of propeller wake wash include clearing pack ice and broken ice from offshore installations and shipping channels. A numerical model of a propeller wake has been developed to simulate the effect of the wake, or jet, on ice pieces floating on the water surface. The propeller jet was modeled using empirical equations derived from previous experiments. Model predictions are compared to experimental results of pack ice subjected to propeller wake wash. The analysis shows that this model can be used to simulate the clearing of pack ice. It has potential to be applied to model ice management operations.

ACKNOWLEDGEMENTS

I would like to extend my gratitude to all those who have helped me in the completion of this Master's thesis. First and foremost, I would like to thank my supervisor's Dr. Brian Veitch and Dr. Ayhan Akinturk for their invaluable help and guidance as my advisors throughout my time at Memorial University of Newfoundland. Besides my supervisor's, I would like to thank Dr. Jungyong Wang and Dr. Rocky Taylor for their encouragement, and insightful comments during the bi-weelky meetings. I extend my thanks to National Research Council of Canada's Ocean, Coastal and River Engineering (NRC-OCRE) Portfolio for providing the office space and particularly Allison Kennedy and António Simões Ré for the support provided during my term at NRC-OCRE. I would like to thank MITACS and Virtual Marine Technology (VMT) particularly Randy Billard for providing the opportunity to do an internship, which was a great learning experience. Finally, I would like to thank my parents for their prayers, inspiration and support throughout my graduate studies.

Table of Contents

List of Tables

List of Figures

Nomenclature

a	Multiplier for jet expansion near free surface
$b_{(X/Dp)}$	Radius of jet at a downstream location = X/Dp
$B_{(X/Dp)}$	Half–width of plume intersection with free surface
CFD	Computational Fluid Dynamics
D_p	Propeller Diameter (m)
D_h	Hub Diameter (m)
J	Advance coefficient (Dimensionless)
h	Depth of immersion of propeller from free surface
K_t	Propeller Thrust Coefficient at J = 0 (Dimensionless)
n	Propeller Rotational Speed (RPS)
N	Blade Number (Dimensionless)
$R_{Max(X/Dp)}$	Position of maximum axial velocity in ZFE (m)
$R_{MaxTangential(X/Dp)}$	Position of maximum Tangential velocity (m)
R_p	Propeller Radius (m)
RPM	Revolutions per Minute
RPS	Revolutions per Second
V_0	Efflux Velocity ($m.s^{-1}$)
$V_{Axial(X/Dp,Y/Rp)}$	Axial velocity at a downstream location = X/Dp and radial location = Y/Rp ($m.s^{-1}$)

$V_{MaxAxial}$	Maximum value of Axial velocity
$V_{MaxAxial(X/Dp)}$	Maximum value of Axial velocity at a downstream location = X/Dp
$V_{MaxTangential}$	Maximum value of Tangential velocity
$V_{MaxTangential(X/Dp)}$	Maximum value of Tangential velocity at a downstream location = X/Dp
V_P	Propeller tip Velocity ($m.s^{-1}$)
$V_{Tangential(X/Dp,Y/Rp)}$	Tangential velocity at a downstream location = X/Dp and radial location = Y/Rp ($m.s^{-1}$)
X	Axial Distance downstream of the propeller (m)
Y	Radial Distance from the axis of the propeller (m)
Z	Vertical Distance from the axis of the propeller
ZEF	Zone of Established Flow
Z_n	Number of Propeller Blades (Dimensionless)
θ	Jet spread angle
ζ	Efflux coefficient
μ	Kinematic viscosity of Water ($kg.s^{-1}.m^{-1}$)
ρ	Density of Water ($kg.m^{-3}$)

1 CHAPTER 1 - INTRODUCTION

1.1 AIM

The subject of this thesis is the clearing of pack ice or broken ice pieces, when the ice is subjected to the propeller wash behind a ship. The aim is to understand the physical phenomena behind the process and to develop a mathematical model that simulates the real time clearing of pack ice subjected to the propeller wake wash from a ship. The model predicts the velocities in the wake created by a ship's propeller and the motion of the pack ice in response to it. This model can be used to simulate the clearing of pack ice in a real time simulator.

1.2 ICE MANAGEMENT

With growing demands for oil, exploration and extraction operations of petroleum in the Arctic and nearby ice covered waters is under way. Arctic and sub-Arctic waters pose a challenge for the offshore industries, particularly in dealing with environmental conditions like extreme temperatures and ice conditions. To obtain drilling exploration permits in Arctic waters, operators are required to show regulatory bodies how operational challenges in these extreme environments will be addressed. This has increased the need for improved knowledge and techniques on ice management in these conditions. Effective ice management can significantly increase the number of days in which the drilling operations can be carried out by preventing interruption during summer ice incursions and allowing extension into the ice-covered periods (Hamilton 2011). This extended drilling period provided by ice management acts as an economic driver for

improving existing ice management techniques. Figure 1 below illustrates the extended operational time achieved using ice management when compared to an operation without ice management.

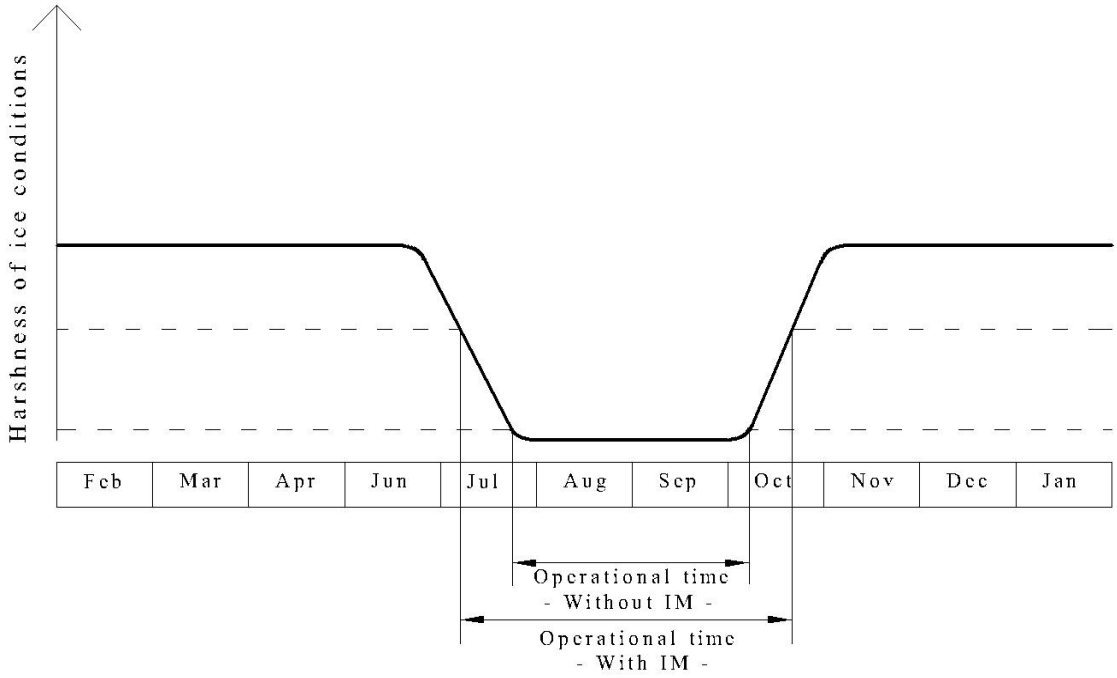

Figure 1. Illustration of extended operational time achieved using Ice Management

(Adapted from Veitch, 2014 in personal communication)

According to International Standards Organisation, ice management involves operational procedures that can reduce global and local ice loads. Ice management can include ice detection, tracking, forecasting, threat evaluation, icebreaking, ice clearing, ice alert procedures and offshore structure disconnection procedures (ISO 2010). Ice management requirements for any new drilling operations or production concepts should be evaluated at an early stage and should be made an integrated part of the design process (Eik 2008).

The ice conditions experienced by a drilling or production platforms can vary widely. In most cases, it is expected to be relatively small ice floes rather than large unbroken sheets of ice or ice-bergs. In case of bigger ice floes or ice sheets, ice breakers can be used to break up them into smaller pieces before they reach offshore drilling or exploration operations. The ice can be pack ice that has drifted under the natural action of wind and ocean current, or it can be managed ice, created by the action of icebreakers upstream of the petroleum installation (Edmond et al. 2011). Propeller wake wash can be used for clearing pack ice and broken ice from offshore installations and shipping channels. The propeller wash is directed towards the ice floes or ice pieces, which are thereby cleared away from the offshore structures or shipping channels. Figure 2 below shows the schematic diagram of using propeller wake to clear ice.

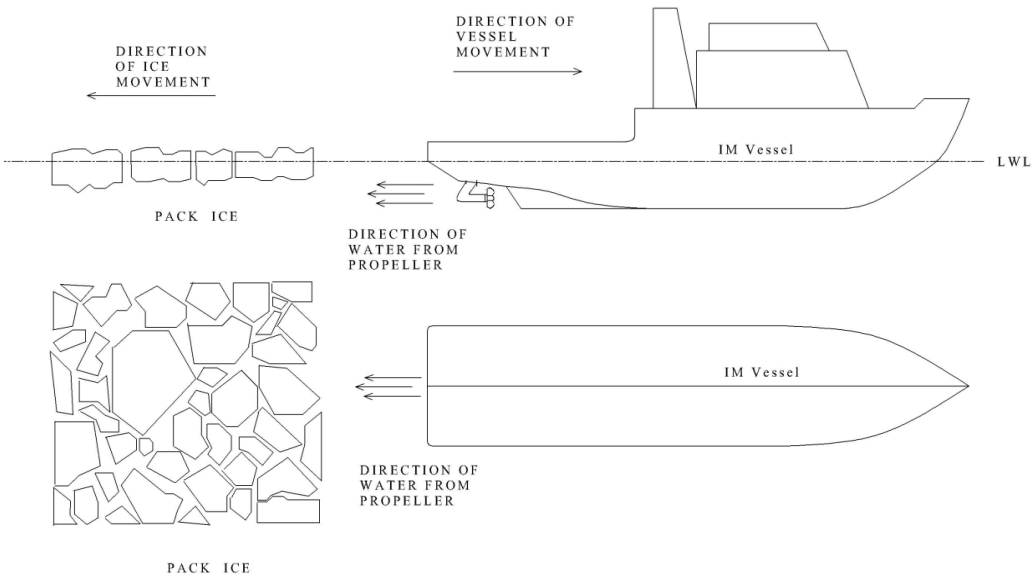

Figure 2. Schematic of Using Propeller Wake to Clear Ice

1.3 LITERATURE REVIEW

A review of the small ice mass management systems for offshore Newfoundland by Anderson et al. (1986) and a more recent review by Crocker et al. (1998) studied the past, prevailing and conceptual techniques of ice management. In these studies, propeller wash was identified as one of the successfully used management techniques for small ice masses. Anderson et al. (1986) stated that it is effective only for ice masses in close proximity to the drilling unit, needs skilled boat handling and its effectiveness is reduced in rough seas.

Earlier studies on ice management were focused on accessing the ice loads encountered by a moored platform and the platform's station keeping performance. Pilkington et al. (1988) discussed the full scale performance of the moored drilling platform Kulluk based on its 3 years operating in the Canadian Beaufort sea and compared it with its model tests and predicted performance. Wright (1998) studied the feasibility of moored vessel station keeping in the pack ice conditions, waves, growlers, bergy bits and small icebergs that are encountered on the Grand Banks. Wright (1999) gave a detailed review of data that was available regarding the full scale loads on moored vessels in pack ice. Wright (2000) documented the full scale information that is relevant to the question of moored vessel station keeping in moving pack ice and discussed its implications on the development of floating production systems for Grand Banks pack ice conditions. Comfort (2001) gave a detailed study of model test data of floating production systems to identify overall trends and to make basic comparisons. This study included both managed and ambient ice conditions. Wright (2001) gave a summary of the ice loads

acting on the Kulluk in heavy ice conditions, the variations of ice loads in managed ice with and without effective clearing and as a function of the number of icebreakers used.

A number of studies have focused on the details of particular ice management operations. Hinkel et al. (1998) gave a detailed description of the drilling of the 2 wells – Hammerhead I & II – in the US Beaufort Sea using a drillship, Canmar Explorer II, and its support fleet. The assessment of this operation showed that the offshore exploration in the U.S. Beaufort Sea can be undertaken with effective ice management support. A description of the equipment used, ice environment, ice management and operations for laying down the SALM buoy during the six years of oil extraction at Sakhalin was given by Keinonen (2006 a). It was found that the number of days of oil production was significantly increased by using ice management. Keinonen (2006 b) gave a description of the station keeping operations of the drilling vessel Vidar Viking during coring of soil samples under the polar ice pack in high concentration of multiyear ice. The success of this operation is attributed to effective ice management and marine operations using two ice management vessels - Sovetskiy Soyuz and Oden. The more powerful icebreaker - Sovetskiy Soyuz - was positioned farther upstream of the operation and broke down large floes into smaller ice floes. The less powerful icebreaker - Oden - broke the pre-broken ice floes into even smaller pieces that could pass Vidar Viking and allowed to keep station. He also recommended the use of ships with azimuthing propulsion as ice management vessels for better ice management performance. The ice observations and forecasting techniques used during the same drilling operations in the polar ice pack were discussed in detail by Pilkington et al. (2006). The ice drift measurements were made by

GPS buoys placed on the ice and monitored using helicopters. A simple ice forecast model used during the expedition provided good forecasts in comparison to measurements. A comprehensive review of the operations carried out in ice environments using ice management techniques was made by Eik (2008). This study claimed that the use of ships with azimuthing thrusters significantly improved the ice management performance especially for clearing the ice around a structure. The study also stressed on the importance of evaluating the ice management capabilities at an early stage while planning new operations or during the evaluation of new drilling and production concepts. Edmond et al. (2011) outlined the initial ice and iceberg management plans for the Shtokman Field in the Barents Sea and explained the rationale behind the choices made for ice operations. This more recent review of ice management mentioned the use of azimuthing propeller wake as a means of clearing ice away from offshore structures. Maddock et al. (2011) described the results of full-scale ice management trials conducted in 2009 by Imperial Oil Resources Ventures Limited in the Fram Strait. The results from the trials, together with the simulation work carried out subsequently, helped in developing ice management techniques suited for the Beaufort Sea.

Numerical models focused on various aspects of ice management have also been developed. In some cases, the numerical model predictions were compared to the real time data from the operations discussed above. Barker et al. (2000) did numerical simulations of the moored drilling vessel Kulluk to predict the upper bound force values found from the analysis of Kulluk field data by Wright (1999). Spencer et al. (2009) developed an equation for predicting ice loads due to pack ice on a ship-like structure.

The effects of ice concentration, hull-ice friction coefficient, ice thickness, ice strength and floe size were considered in the development of this equation. Eik and Gudmestad (2010) performed an evaluation of iceberg management systems for an offshore site in the Barents Sea. This study included numerical simulations to obtain maximum ice loads on the offshore structure with and without ice management and found that the maximum load was significantly reduced with ice management. Zhou et al. (2011) and Sayed et al. (2011) both independently developed numerical simulations of interaction between a moored ship and ice and compared model predictions to estimates of forces from previous analysis of field deployment data from the Kulluk. Hamilton (2011) discussed the ice management technique of using two or more icebreakers working upstream to break down the ice floe size before it reaches the petroleum installation. A simulation of the technique was also developed to test the effectiveness of the ships used and their ice management tactics. The paper identified a racetrack pattern to be more effective than circular and orbital patterns for maintaining required channel width near the drill ship.

Anderson et al. (1986), Crocker et al. (1998), Keinonen and Lohi (2000), Eik (2008), Keinonen (2008) and Edmond et al. (2011) list the use of propeller wake as a means of ice management. Keinonen and Lohi (2000) reported full-scale ice management trials on two vessels with azimuthing propellers and showed that azimuthing propellers can be used effectively in managing and clearing sea ice with wake wash. They also reported the use of propeller wake for clearing ridge fields and widening channels. Keinonen (2008) also reported the use of propeller wake for clearing sea ice and ridge fields. He reported on the use of azimuthing propeller wake to create ice free channels

both with and without the presence of a primary ice management vessel. In ice thickness ranging from approximately 0.1 to 1.25 m, azimuth thruster wake was able to create channel widths between 40 and 110m. When aided by a primary icebreaker to break ice floes, they were able to create ice free channels between 30 and 190 m wide in ice ranging from1.9 to 2.7 m thick. The amount of ice coverage, the power required for ice clearing with azimuthing thrusters, and information on sea state and weather conditions were not reported.

Model tests were done by Ferrieri (2012) to identify the factors influencing the effectiveness of propeller wake to clear ice. The test data were analysed using the design of experiments (Montgomery, 2009) methodology and the most important factors affecting the clearing of ice were found to be propeller shaft speed (power) and inclination angle of the propeller.

1.4 SCOPE OF WORK

The focus of this study is to develop a model of propeller wake wash and to apply this model to simulate interaction between the wake wash and ice cover. The development of such a model needs a detailed understanding of the physical phenomena involved in this process. The whole problem can be broken down into three components: 1) model of a deeply submerged propeller jet, 2) model of the interaction between the deeply submerged jet and the free surface of water, and 3) model of ice floe motion due to the action of the propeller jet at the free surface.

The objectives of the thesis are:

1) To understand the basic physics behind the propeller wake wash and ice floe interaction.

2) To mathematically model the three subcomponents required for modeling propeller wake wash and ice floe interaction.

3) To couple the three subcomponent models into a unified propeller wake wash-ice floe interaction model.

4) To validate the results from the model by comparing it to experimental results.

2 CHAPTER 2 - THEORY

2.1 SCOPE

This chapter gives an introduction of the propeller jet-ice floe interaction problem. The problem of propeller jet-ice floe interaction can be broken down in to three sub-models as discussed here: 1) deeply submerged propeller jet, 2) interaction between the deeply submerged jet and the free surface of water, and 3) ice floe motion due to the action of the propeller jet at the free surface. The detailed literature review and the rationale behind the development of each of these sub-models are also discussed in this section.

2.2 INTRODUCTION

The propeller operates by converting shaft torque to produce axial thrust by drawing in water, accelerating it and discharging this water downstream in the form of a turbulent jet. The propeller jet behind the ship with forward speed is influenced by the ship's wave field and wake, making the flow pattern more complex (Hamil, 1987).When the ship is stationary or at low speeds, the ship's wake and wave field are insignificant and can be neglected (Prosser, 1986). The development of the model is based on this assumption of no interaction of ship's wake with propeller wake at lower operational speeds.

When a propeller is deeply submerged in water and is not bounded by any physical obstruction or free surface, the jet can be assumed more or less symmetric about the propeller axis for the modelling in spite of the turbulence present in the jet. The velocity of the jet created by its rotation decays with increasing downstream distance from the face of the propeller and it

starts to entrain water from the surrounding fluid (Hamil, 1987). When the propeller is near the free surface of the water, the jet is restricted by the free surface of water and the interaction gives rise to free surface deformations, such as wave generation and shallow surface currents (Anthony, 1989). When ice floes are present in the turbulent wake of the propeller jet, motions are induced by the forces transferred to them from the water near the surface.

2.3 DEEPLY SUBMERGED PROPELLER JET

A deeply submerged jet is one in which the propeller creating the jet is kept deeply submerged and the generated jet is not influenced by the boundaries of water including the free surface. The velocity magnitude of a propeller jet generated by the rotation of a deeply submerged propeller decays along the longitudinal axis downstream of the propeller (Hamill, 1987; Stewart, 1992; McGarvey, 1996). As the fluid in the jet gradually decelerates downstream of the propeller, the still ambient fluid around the jet accelerates slightly. This is attributed to high viscous shear eddies which induce lateral mixing of the propeller wake (Brewster, 1997).

Albertson et al. (1950) has assumed that the diffusion process is dynamically similar under all conditions. According to Blaauw and Van de Kaa (1978), dynamic similarity requires all the forces at points with the same radial distance from the rotation axis and same section to be the same, and therefore a propeller jet is symmetric if the above condition is true. Actually, the propeller jet is not symmetric owing to the huge amount of turbulence present in it which is confirmed by the experimental measurements. The turbulence is highest at the zone of flow establishment (ZFE), decreases in the zone of established flow (ZEF) and finally the jet reaches self similarity at $80D_p$ downstream (Wygnasnski and Fiedler, 1969), where D_p is the propeller

diameter. For the purpose of this modelling, the turbulence is neglected and the propeller jet is treated as symmetric about the rotation axis. A schematic representation of the propeller jet based on the description of previous researcher is given in Figure 3 below. The propeller jet is shown with velocity distribution profiles downstream of the propeller symmetric about the propeller axis. The velocity profiles one inside the ZFE and the other inside the ZEF is shown.

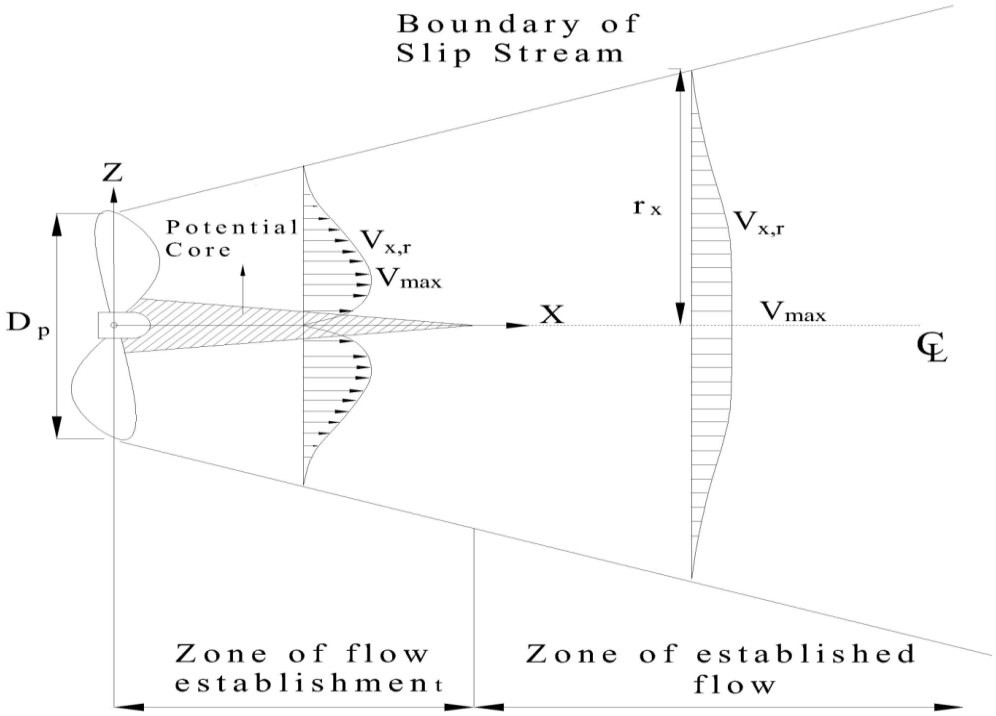

Figure 3. Schematic representation of propeller wake

(After Hamill, 1987 and Albertson et al., 1950)

The development of the propeller jet can be divided into two regions, the zone of flow establishment (ZFE) nearer to the propeller face, and the zone of established flow (ZEF) further downstream (Lam et al. 2011a). In the zone of flow establishment, there is a low velocity core

surrounding the axis of rotation due to the lower thrust generated by the propeller hub (Lam et al 2010). In this zone, water mixes both outwardly with surrounding ambient still fluid and inwardly with water in the low velocity core (McGravey, 1996). Due to this, the axial velocity in the ZFE has two peaks located on either side of the centreline. As the inward mixing progresses downstream of the propeller, a stage is reached where the jet reaches the axis of rotation beyond which the ZEF begins (Situ et al. 2010). In the ZEF, the flow will only be mixing outwardly and there is only one velocity peak located at the axis of rotation (McGarvey 1996). The extent of ZFE was a subject of interest to researchers: experimental results on propeller jet analysis yielded different lengths for ZFE. Stewart (1992) defined the length of ZFE by the position where the two peaks combine into one peak position at the rotation axis. The length of ZFE was found to vary between $2D_p$ (Hamill (1987)) and $3.68D_p$ (Lam et al. (2010)). A value of $3.25D_p$ measured by Stewart (1992) was used for the present modeling.

The resultant propeller jet velocity at any point inside the jet can be broken down into three components: axial, tangential and radial. The main contributor of propeller jet velocity is the axial component, which is followed by tangential and radial components (Lam et al. 2011). Experiments carried out by Lam et al.(2010) determined the maximum percentages of these components when compared with efflux velocity. Efflux velocity is defined as the maximum velocity at the face of the propeller (Fuehrer and Romisch, 1977). Experimental measurements show that the magnitude of maximum axial velocity is equal to the efflux velocity. The magnitude of maximum tangential velocity as measured by Lam et al. (2010) was 82 % of the efflux velocity. The axial decay and the radial positions of the maximum values of these tangential components were also recorded. The magnitude of the tangential component decreases

to 2 % by the time it reaches a downstream location of $X=6.32\ D_p$ and so this component was neglected for locations farther downstream of the propeller. The magnitude of maximum radial velocity as measured by Lam et al (2010) was only 14 % of the efflux velocity and so was not considered for modelling. A schematic representation of the axial, tangential and radial velocities inside the plume and the coordinate system is given in Figure 4 below.

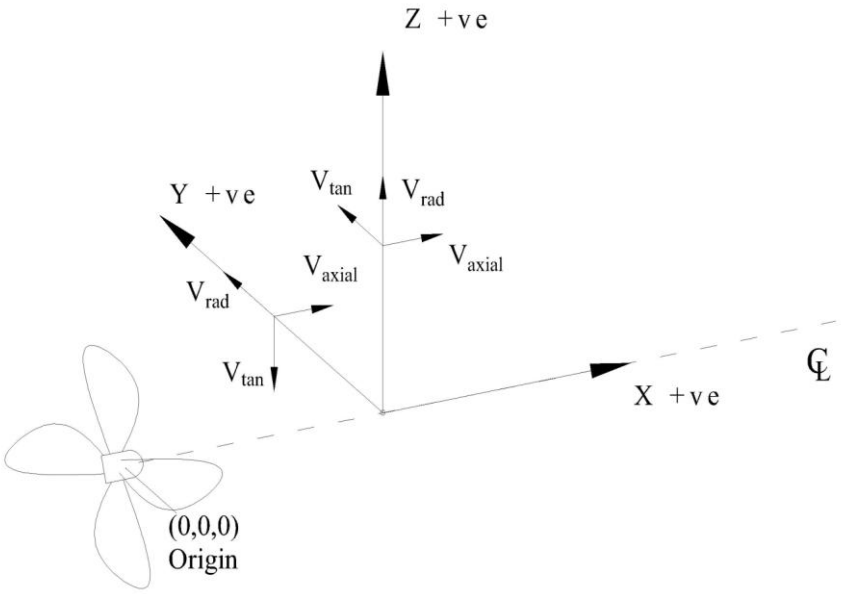

Figure 4. Co -ordinates system and velocity component directions

The details of efflux velocity, axial velocity, tangential velocity and the jet spread radial angle are discussed below.

2.3.1 Efflux Velocity (V_0)

Efflux velocity is defined as the maximum velocity at the face of the propeller. The axial and tangential velocities and their decay downstream of the propeller are dependent on the efflux

velocity and calculated from it. Therefore, the estimation of the efflux velocity is important for prediction of velocities. The empirical equation for efflux velocity proposed by Fuehrer and Romisch (1977) based on axial momentum theory is given by

$$V_0 = 1.59 n D_p \ K_t^{0.5} \qquad (2.1)$$

Fuehrer and Romisch (1977)

where V_0 is the efflux velocity ($m.s^{-1}$)

D_p is the propeller diameter (m)

K_t is the propeller thrust coefficient at $J = 0$ (Dimensionless)

n is the shaft speed

This equation has been used by the majority of researchers to predict the efflux velocity due to its strong theoretical support from axial momentum theory. The researchers Hamill (1987), Stewart (1992), McGarvey (1996) tried to refine this equation using experimental investigations. A comparison of the efflux velocities predicted by all these investigators to the measured value of efflux velocity for a propeller was made by Lam et al. (2010). The measured value was higher than most of the values and it was found that the equation by Fuehrer and Romisch (1977) made the closest prediction when compared to all the other prediction equations. Hence the equation derived from axial momentum theory is used here in the model for the prediction.

According to Hamill (1987), the radial location of efflux velocity ($R_{Max(X/Dp\ =\ 0)}$) is the radial distance from the propeller axis where the maximum thrust occurs. See Figure 5 below for the schematic representation of the location of efflux velocity. The radial locations proposed by different researchers were different and were found to depend on the propeller geometries. The

equation proposed by Lam et al. (2010) based on experimental result was used in the present model.

$$R_{Max(X/Dp=0)} = 0.53R_p \quad (2.2)$$

where R_p is the radius of the propeller

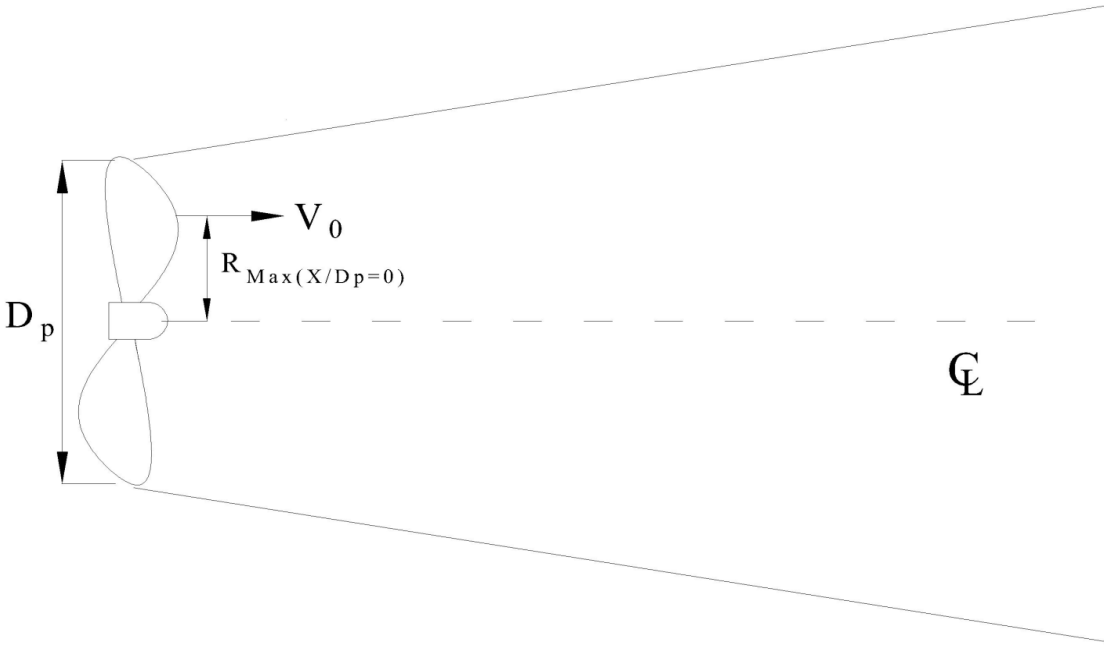

Figure 5. Location of efflux velocity

2.3.2 Axial Component of Velocity

The main contributor of the resultant velocity at any point in the propeller jet is the axial component. This is followed by the tangential and radial components (Lam et al. 2010). The maximum axial velocity ($V_{MaxAxial}$) is located at the face of the propeller jet and its magnitude is equal to the efflux velocity. This is given by

$$V_{MaxAxial} = V_0 \quad (2.3)$$

(Lam, 2011b)

where V_0 is the efflux velocity

The jet velocity decays along the longitudinal axis downstream of the propeller and follows a distribution across the cross-section of the jet depending on its downstream location. The equation for predicting the decay of maximum axial velocity at a downstream location = X/D_p ($V_{MaxAxial(X/Dp)}$) is given below:

$$\frac{V_{MaxAxial(X/Dp)}}{V_{MaxAxial}} = 1 - 0.1592\frac{X}{D_p} \quad (2.4)$$

for $0 <= X/D_p < 3.25$ (Lam, 2011b)

$$\frac{V_{MaxAxial(X/Dp)}}{V_{MaxAxial}} = 0.638 \times e^{-0.097\frac{X}{Dp}} \quad (2.5)$$

for $3.25 <= X/D_p <= 16$ (Hashmi, 1993)

$$\frac{V_{MaxAxial(X/Dp)}}{V_{MaxAxial}} = 0.638 \times e^{-1.552} \times e^{-\frac{(x-16Dp)^2}{(25Dp)^2}} \quad (2.6)$$

for $16 < X/D_p <= 50$

The equations for decay in the ZFE (i.e. up to X/D_p = 3.25) was taken from Lam (2011b) and subsequent decay up to X/D_p = 16 was taken from Hashmi (1993). These equations were developed based on experimental measurements. The limitations of these equations are that they were made based on test results from a single propeller run at a particular shaft speed. Equations for subsequent decay beyond X/Dp = 16 were not available from previous test results. Johansson

et al. (2006) specified that the downstream axial velocity falls rapidly from 10% of the free stream velocity at $x/D_p=10$ to approximately 2% at $x/D_p=50;$ therefore a top hat profile which gradually decreases to 2 % of maximum axial velocity was assumed in the model.

The distribution of axial velocity at any cross-section downstream is dependent on the downstream location within the propeller jet. One of the conclusions of the experimental results by Lam et al. (2010) was that the radial position of maximum axial velocity (in this case $0.53R_p$) at each downstream location remains the same from the propeller face until the end of ZFE, following which the position drops to the propeller axis. This immediate drop in the radial position of maximum axial velocity at the transition from ZFE to ZEF is arbitrary and unrealistic. A modified version in which this location linearly decreases from its maximum value at the propeller face to zero at the transition from ZFE to ZEF was assumed for the developed model. The position of the maximum axial velocity at the propeller face $R_{Max(X/Dp=0)}$ was taken as $0.53R_p$, which decreases linearly in the propeller wake until it coincides with the propeller axis at the end of ZFE (at X/D_p = 3.25). Farther downstream at X/D_p > 3.25, the position of the maximum axial velocity remains at the centerline. See Figure 6 below for the schematic representation of the radial position of the maximum axial velocity and radial distribution of the axial velocity used in the present model. For further detail on the radial distribution profile, see page 21.

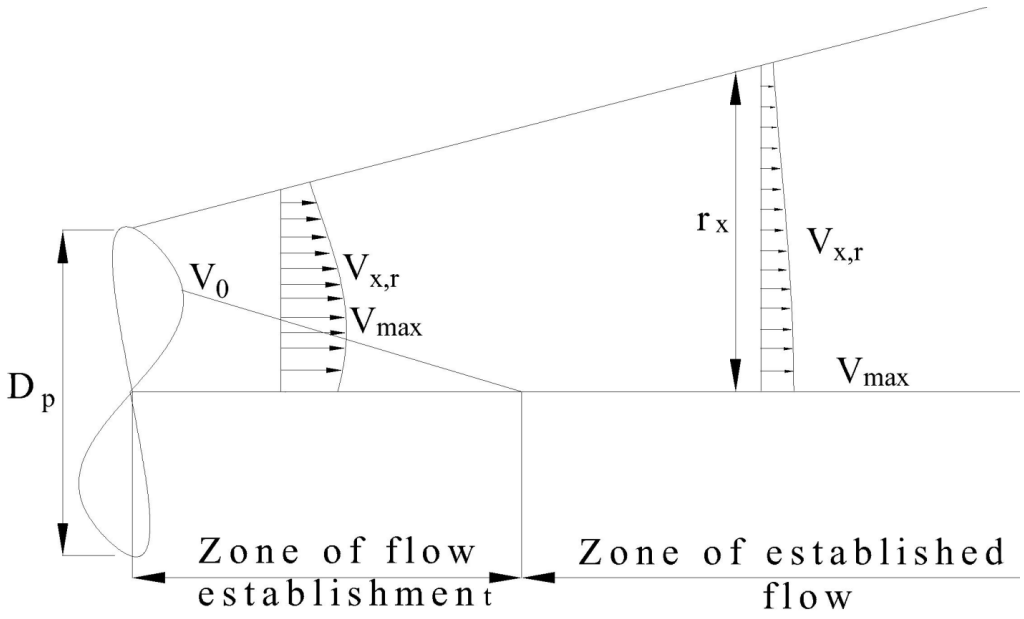

Figure 6. Schematic representation of the position of the maximum axial velocity used in modeling.

2.3.3 Tangential Component of Velocity

The tangential component of velocity is the component which gives the rotating effect to the propeller jet. The maximum value of the tangential component and its decay is discussed below. The maximum value of tangential component $V_{MaxTangential}$ was measured as 82 % of the efflux velocity by Lam et al. (2010) in their experiment and so it is the second largest contributor to the resultant velocity filed. Prosser (1986) approximated the maximum tangential velocity to be 30% of the efflux velocity, which according Lam et al. (2010) was a limitation of the measuring system used at that time.

The decay of the tangential component downstream of the propeller was at a much higher rate when compared to the axial component. It was seen from measurements by Lam et al. (2010) that the magnitude of the tangential component reached 2 % of $V_{MaxTangential}$ at X/D_p =

6.32. Figure 7 below shows the axial decay and radial location of the maximum tangential velocity at a downstream location as recorded by Lam et al. (2010). The tangential component is neglected after X/D_p = 6.32.

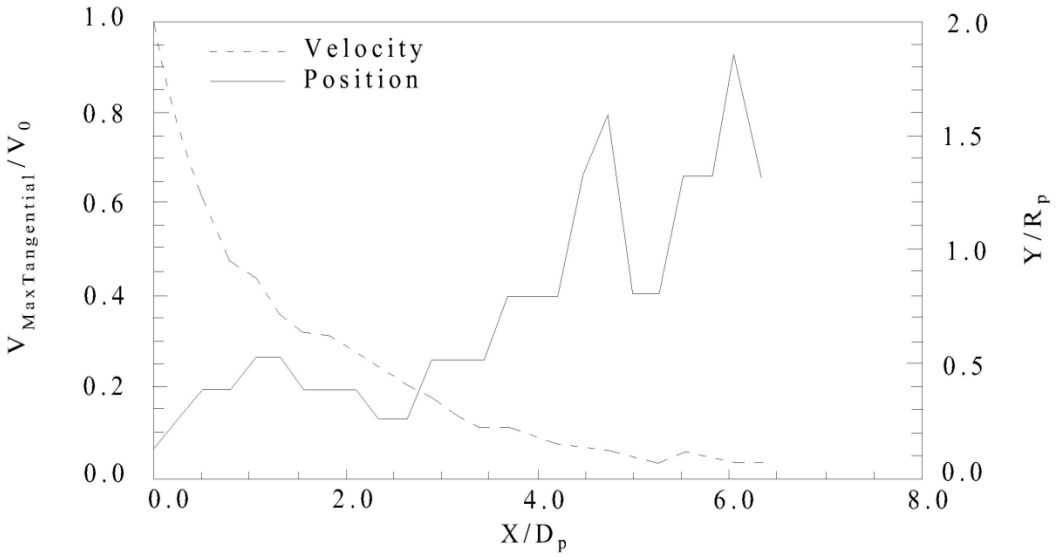

Figure 7. Axial Decay and Radial Position of Maximum tangential velocity

(Adapted from Lam 2011)

The equations for predicting the maximum value of tangential component $V_{MaxTangential(X/Dp)}$ at a distance downstream was also given by Lam et al. (2011). These equations are given below:

$$\frac{V_{MaxTangential(X/Dp)}}{V_{MaxTangential}} = 0.9749 - 0.6492\frac{X}{D_p} \qquad (2.7)$$

used from 0<= X/D_p <0.79(Lam, 2011b)

where $V_{MaxTangential}$ is the maximum value of tangential velocity.

$$\frac{V_{MaxTangential(X/Dp)}}{V_{MaxTangential}} = 0.7031e^{-0.4998\frac{X}{Dp}} \quad (2.8)$$

used from 0.79<= X/D_p <6.32(Lam, 2011b)

where $V_{MaxTangential}$ is the maximum value of tangential velocity.

The radial position of maximum tangential velocity at a downstream location was modeled using the experimental results by Lam et al. (2011b). The experimental data in Figure 7 were used to develop a set of interpolation equations for the present model for radial positions of maximum tangential velocity.

2.3.4 Jet half-width and radial spread angle

In the previous sections, the equations for predicting the velocities and their decay inside the plume were given. In this section, the radial expansion of the plume and its distribution after it is generated by the propeller is discussed.

The jet generated by the propeller expands radially once it leaves the propeller and this radial expansion of the jet can be assumed more or less linear once the jet achieves steady state after a number of revolutions. In Figure 8 below, a propeller jet expanding linearly with a jet spread angle θ is shown. The radius of the jet at which the velocity becomes half the centerline velocity at a downstream location can be calculated from the angle θ at which it is expanding and is given by

$$b_{(X/Dp)} = \frac{D_p}{2} + tan\theta\, X \quad (2.9)$$

where D_p is the diameter of propeller

X is the downstream distance

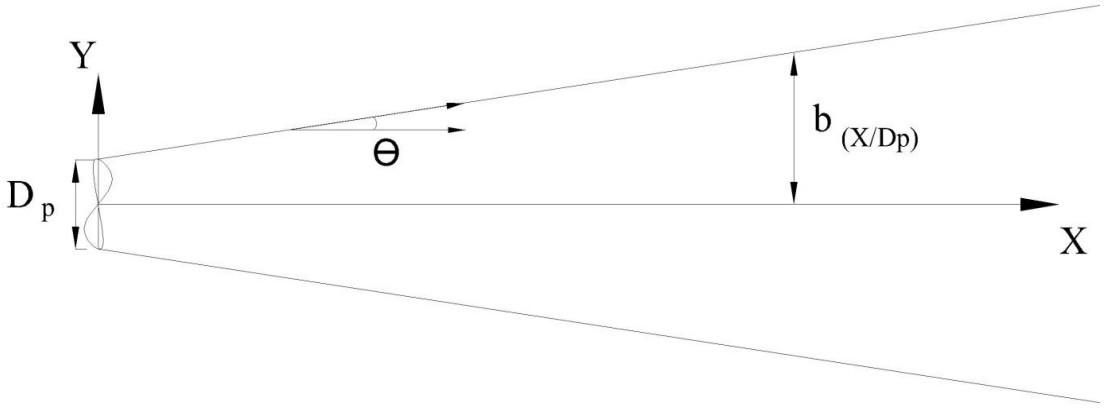

Figure 8. Schematic representation of the radial expansion of jet.

The jet spread angle and the distribution equation for velocity based on a Guassian distribution was discussed by Loberto (2007). In this study, the jet spread angle was found to be 8.2^0 for 3000 rpm with the propeller used. For the purpose of modeling, the jet spread angle was assumed to remain constant at 8.5^0 simplifying equation (2.9) to

$$b_{(X/Dp)} = \frac{D_p}{2} + 0.15\,X \qquad (2.10)$$

Where D_p is the diameter of propeller

X is the downstream distance

The use of Gaussian distribution to define the velocity profiles at downstream locations is widely used in the case of round jets and is discussed by Lee and Chu (2003). The Gaussian distribution discussed by Loberto (2007) with some slight modification is applied to the model and the equations based on their location in ZFE and ZEF are given below:

$$\frac{V_{(X/Dp\ ,\ Y/Rp)}}{V_{(X/Dp)}} = e^{-0.69\frac{(Y-R_{Max(X/Dp)})^2}{(b_{(X/Dp)})^2}} \quad (2.11)$$

in ZFE.

$$\frac{V_{(X/Dp\ ,\ Y/Rp)}}{V_{(X/Dp)}} = e^{-0.69\frac{(Y)^2}{(b_{(X/Dp)})^2}} \quad (2.12)$$

in ZEF.

The same distribution is assumed for both axial and tangential velocities.

2.4 INTERACTION BETWEEN THE DEEPLY SUBMERGED JET AND THE FREE SURFACE OF WATER

The previous sections talked about the characteristics of a deeply submerged propeller jet without any interaction with the free surface. In this section, the case of a ship propeller where the propeller jet is modified by the free surface is discussed. A simple demonstration of the plume intersecting a free surface is discussed showing geometric constraints due to the free surface, following which the actual modification happening near the free surface is explained based on experimental findings by previous researchers.

Figure 9 below shows a propeller jet intersecting with the free surface assuming no modification occurs. When the plume simply intersects with free surface of water and no modification is assumed, a region on the water surface having a half-width of $B_{(X/Dp)}$ is created. In the plan view shown in the figure below, this region is represented by the parabolic curve drawn as dotted line inside the radial spread of the jet. From the profile view, it can be seen that the velocity profile is truncated at the free surface after the propeller jet starts hitting the free surface.

The sectional view shows the volume lost above the water surface at a representative section in a free surface intersecting plume.

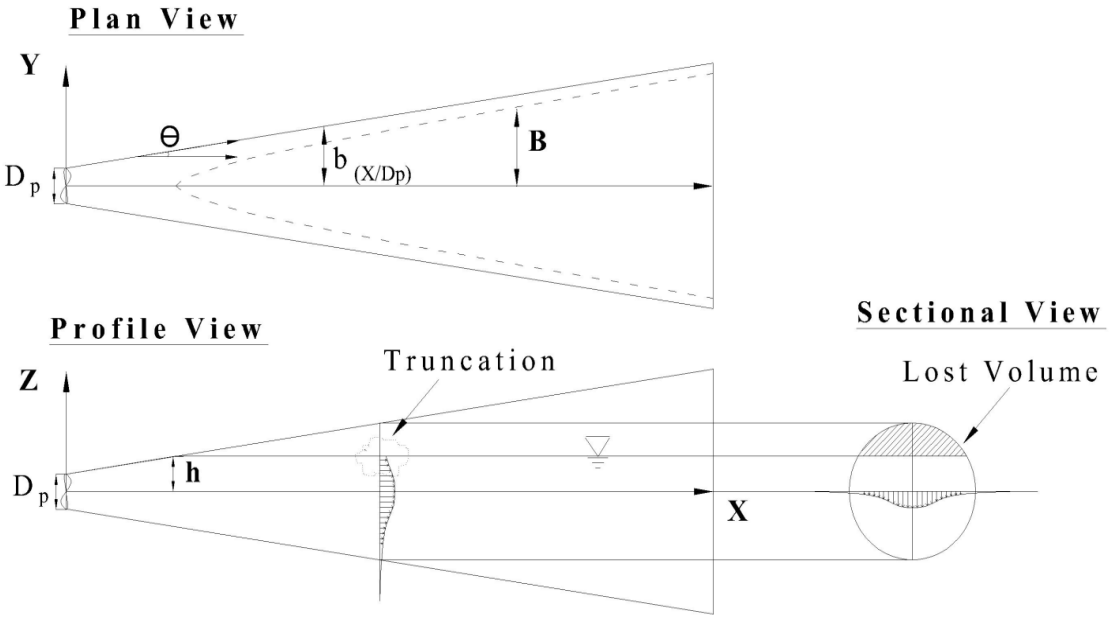

Figure 9. Schematic representation of propeller plume intersecting the free surface

In reality, to account for the lost volume, when a jet interacts with the free surface it gives rise to free surface deformations. This problem was experimentally studied independently by Bernal and Madina (1988) as well as Anthony (1990). The findings of these experiments relating to turbulent jet/free-surface interaction are discussed below.

When a jet is kept at a location near the free surface, the jet expands more or less symmetrically about its centerline axis downstream until it starts hitting the free surface. As soon as the jet hits the free surface, it give rise to free surface deformation due to the interaction of

turbulence in the underwater jet with the free surface. The important aspect of this interaction is the generation of waves and surface current.

The generation of surface current due to the interaction of the jet with the free surface was studied by Anthony (1990). The generation of surface waves was also noted. A round jet kept at a depth of two diameters below the free surface was studied. According to him, as soon as the jet started to interact with the free surface, surface activity was seen near the jet centerline and it was only near the edges of this active region that the surface became identifiable as outward travelling waves. The jet velocities were recorded at various locations downstream of the jet. At downstream location near to the beginning of the interaction, the flow near the edges of the submerged jet was directed inward except at the free surface where it shows a small outward component. After a few propeller diameters downstream, the surface current becomes apparent and is visible as a shallow current near the free surface. Further downstream, the surface current is well established and it can be seen that the surface current extends laterally to beyond twice the width of the jet flow just beneath it. Thus, the surface current becomes the dominant feature of the flow. The surface current was modeled based on the data acquired from Anthony (1990) and a modification was applied to the location at which the jet starts hitting the free surface. A larger surface current width was also assumed for a propeller jet compared to a round water jets. The application of the surface current in the model is discussed below.

The data of surface current generated by the round jet from Anthony's (1990) experiment was re-plotted at the free surface for the given X/D_p locations. In Figure 10 below, the origin is located at the point where the jet started hitting the free surface. The plot of velocity contour 0.5

obtained by normalizing the velocity at the free surface with the centerline velocity is shown as a half-plan view. The trend line for the velocity contour 0.5 was also plotted and an equation $Y = 0.22 \times X + 0.1$ was obtained.

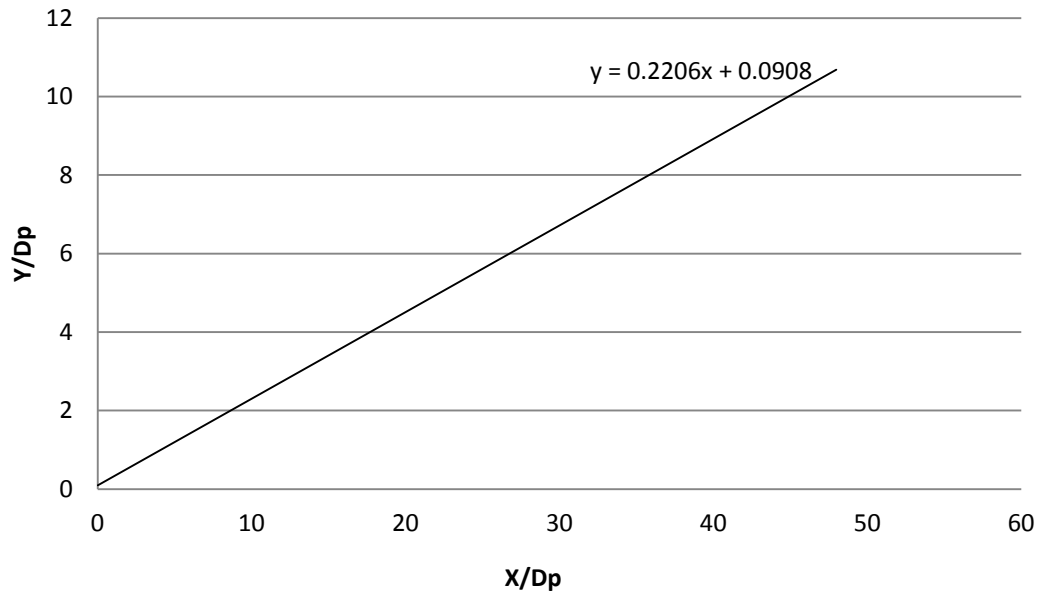

Figure 10. Half-plan view of the velocity contour 0.5 on free surface after jet/free-surface interaction. (Adapted from Anthony, 1990)

The trend line equation indicates the lateral expansion of the plume on the free surface and hence the deep water jet expansion equation 2.10 can be modified to account for this change. Considering the factor that the experiments were conducted for a round jet, an increased expansion multiplier of 0.32 was assumed for a propeller instead of 0.22 for the round jet. The model can be further improved by conducting future experiments to confirm this assumption of increased expansion for propeller. Equation 2.10 can be rewritten as shown below for the jet/ free- surface interaction problem:

$$b_{(X/Dp)} = \frac{D_p}{2} + 0.32\,X \qquad (2.13)$$

where D_p is the diameter of the propeller.

The generation of waves was studied by Bernal and Madina (1988), who attributed the wave generation to large scale vortical motion moving underneath and approaching the surface, initially deforming it and eventually breaking the surface. They found that the wave traveled at around 40^0-60^0 away from the jet centerline depending on the Reynolds number. This type of interaction is important because it imparts momentum to the surface and results in associated mass transport (Bernal and Madina, 1988). The presence of surface current layer was not reported or measured during his experiments.

The effect of surface waves was incorporated in the present model by assuming a y-component equal to 5 percent of the maximum tangential velocity to account for the lateral clearing of the ice pieces. This needs to be studied in more detail from future experiments so that the velocity magnitude and direction of the waves generated from the interaction of the jet with the free surface can be modeled correctly.

2.5 DYNAMICS OF ICE FLOE MOTION

For an ice floe drifting under the action of propeller jet the only force acting on the floe would be the water drag (F_W). When a propeller jet is directed at the ice floe, the floe will drift under the action of flow created by the propeller jet. The effects of ocean waves and currents are neglected. With these forces, the equations of motion considered for the ice floe can be written as

$$Ma = F_W \qquad (2.14)$$

where M is the ice floe's mass and a is the acceleration

3 CHAPTER 3-DEVELOPED MODEL AND EQUATIONS USED

The previous chapter presented an introduction to the propeller jet, equations from the literature used in developing a propeller jet, its interaction with the free surface of water, and ice floe motion. In this chapter, the modelling approach and the data flow within the model are explained with help of a flow chart. The equations used in the numerical model are also given.

3.1 METHODOLOGY

The numerical model of propeller jet can be used to predict the velocity at any point inside the jet. The input parameters for making a velocity prediction from the model are propeller diameter (D_p), thrust coefficient (K_t) and shaft speed (n). Using these parameters, the efflux velocity (V_0) is calculated. Based on the location within the jet or on the free surface, the radial expansion of the plume ($b_{(X/Dp)}$) is calculated. From the value of the efflux velocity, the maximum values of axial and tangential components are calculated by using the corresponding equations. The decay of the axial and tangential velocities is then calculated. By giving the longitudinal and radial position at any point within the plume, the magnitude of the axial and tangential velocity at corresponding position can be obtained.

The location of the intersection of the plume with the free surface is calculated based on the depth at which the propeller is placed and the radial expansion of the underwater jet. From the point of intersection, the intersection model of the jet is used in predicting the velocities near the water surface. An increased radius of expansion is assumed near the free surface. Based on the location of ice floes, the velocities at the respective positions are applied to the model and the

motion of the ice floes is determined. The above process is represented as a flowchart in Figure 11 below.

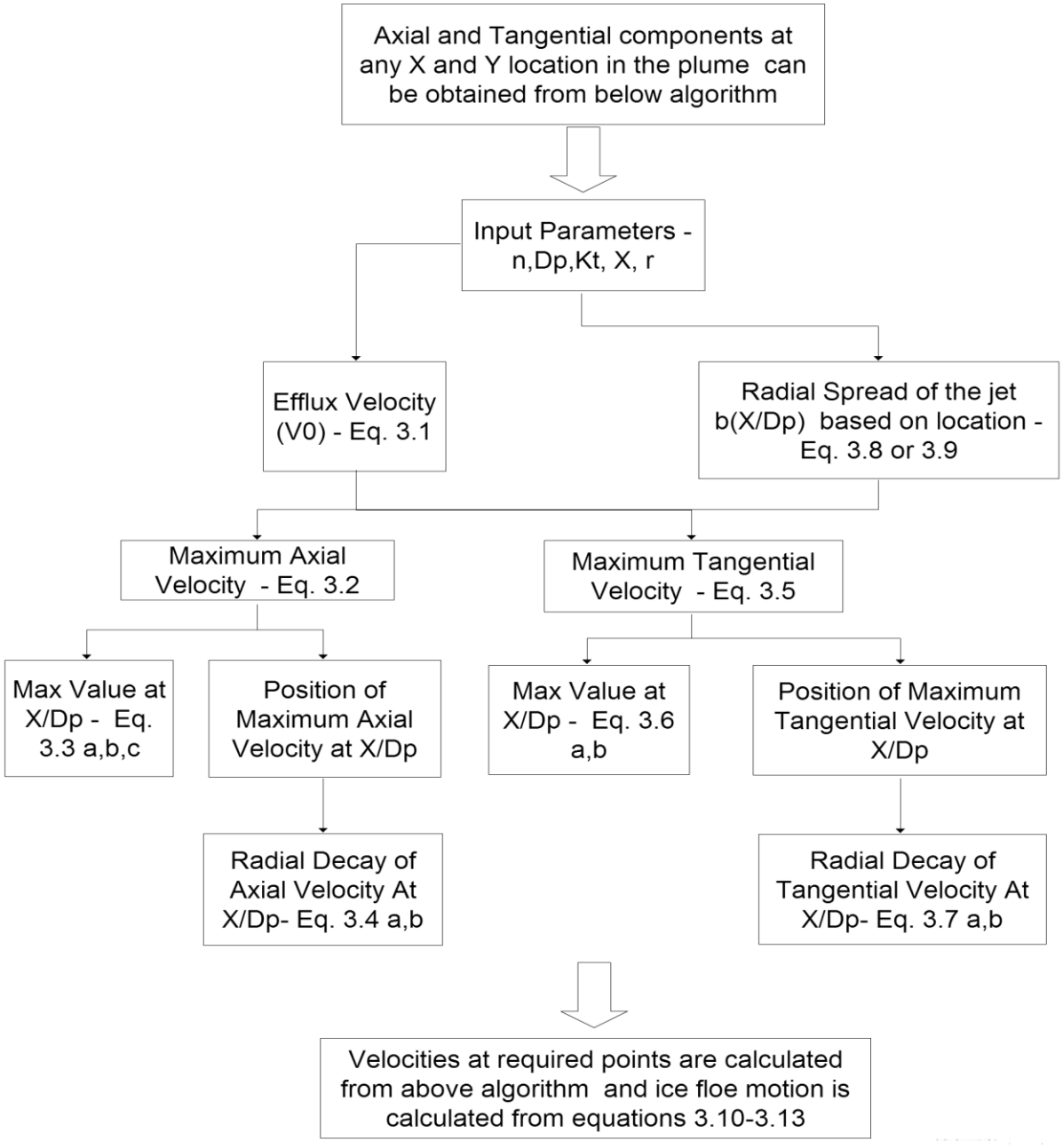

Figure 11. Modeling Method

3.2 DEEPLY SUBMERGED PROPELLER JET

3.2.1 Efflux Velocity

The equation for efflux velocity used in the model is given by

$$V_0 = 1.59 n D_p \ K_t^{0.5} \quad (3.1)$$

(Fuehrer and Romisch, 1977)

where V_0 is the efflux velocity (m.s^{-1})

D_p is the propeller diameter (m)

K_t is the propeller thrust coefficient at $J = 0$ (Dimensionless)

3.2.2 Axial component

The equations used for predicting the maximum value of axial velocity is given by

$$V_{MaxAxial} = V_0 \quad (3.2)$$

(Lam, 2011b)

where V_0 is the efflux velocity

The equation used in the model for predicting the decay of the maximum axial velocity along the propeller axis is given below:

$$\frac{V_{MaxAxial(X/Dp)}}{V_{MaxAxial}} = 1 - 0.1592 \times \frac{X}{D_p} \quad (3.3\ a)$$

used from $0 \leq X/D_p < 3.25$ (Lam, 2011b)

$$\frac{V_{MaxAxial(X/Dp)}}{V_{MaxAxial}} = 0.638 \times e^{-0.097\frac{X}{Dp}} \quad (3.3\ b)$$

used from $3.25 \leq X/D_p \leq 16$ (Hashmi, 1993)

$$\frac{V_{MaxAxial(X/Dp)}}{V_{MaxAxial}} = 0.638 \times e^{-1.552} \times e^{-\frac{(x-16Dp)^2}{(25Dp)^2}} \qquad (3.3\ c)$$

used from $16< X/D_p \leq 50$ (assumed to obtain a top hat profile having a value of around 2 % value at $50D_p$).

The decay of the axial components in the radial direction is modeled using the equations given below:

$$\frac{V_{MaxAxial(X/Dp,Y/Rp)}}{V_{MaxAxial(X/Dp)}} = e^{-0.69\frac{(Y-R_{Max(X/Dp)})^2}{(b_{(X/Dp)})^2}} \qquad (3.4\ a)$$

used from $0\leq X/D_p < 3.25$ (Gaussian distribution based on Lee and Chu (2003) and Loberto (2007))

$$\frac{V_{MaxAxial(X/Dp,Y/Rp)}}{V_{MaxAxial(X/Dp)}} = e^{-0.69\frac{Y^2}{(b_{(X/Dp)})^2}} \qquad (3.4\ b)$$

used from $3.25\leq X/D_p \leq 50$ (Gaussian distribution based on Lee and Chu (2003) and Loberto (2007)).

3.2.3 Tangential component

In the model, the equation used for calculating the maximum value of tangential component $V_{MaxTangential}$ is given by

$$V_{MaxTangential} = 0.82V_0 \qquad (3.5)$$

(Lam, 2011b)

As discussed in the previous chapter, the magnitude of tangential component decreases to 2% of the maximum value of the tangential component $V_{MaxTangential}$ and hence was not considered in the model for downstream distances greater than $6.32D_p$.

The equations for predicting the maximum value of the tangential component $V_{MaxTangential_{(X/Dp)}}$ at a distance downstream used to make the present model is given by

$$\frac{V_{MaxTangential(X/Dp)}}{V_{MaxTangential}} = 0.9749 - 0.6492 \times \frac{X}{D_p} \qquad (3.6\text{ a})$$

used from $0 \leq X/D_p < 0.79$ (Lam, 2011b)

where $V_{MaxTangential}$ is the maximum value of tangential velocity

$$\frac{V_{MaxTangential(X/Dp)}}{V_{MaxTangential}} = 0.7031 \times e^{-0.4998\frac{X}{Dp}} \qquad (3.6\text{ b})$$

used from $0.79 \leq X/D_p < 6.32$ (Lam, 2011b)

where $V_{MaxTangential}$ is the maximum value of tangential velocity.

The radial decay of the maximum value of the tangential component $V_{MaxTangential(X/Dp)}$ was assumed and is given by

$$\frac{V_{MaxTangential(X/Dp,Y/Rp)}}{V_{MaxTangential(X/Dp)}} = e^{-\frac{(Y-R_{MaxTangential(X/Dp)})^2}{(b_{(X/Dp)})^2}} \qquad (3.7)$$

used from $0 \leq X/D_p$ <6.32 (assumed a top hat profile with maximum value at $R_{MaxTangential(X/Dp)}$),

where $b_{(X/Dp)}$ is the radius of jet at a downstream location = X/D_p and $R_{MaxTangential(X/Dp)}$ is the radial position of maximum tangential velocity.

3.2.4 Jet radial spread

The radius of the jet b at any downstream distance X for the present case is assumed to expand linearly by the relation given below:

$$b_{(X/D_p)} = \frac{D_p}{2} + 0.15\,X \qquad (3.8)$$

where D_p is the diameter of propeller.

3.3 INTERACTION OF THE PROPELLER JET WITH FREE SURFACE

The radius of the jet b at any downstream distance X at the free surface after the plume starts interacting with the free surface is given below:

$$b_{(X/D_p)} = \frac{D_p}{2} + 0.32\,X \qquad (3.9)$$

where D_p is the diameter of propeller.

3.4 DYNAMICS OF ICE FLOE MOTION

The motions of the ice floes based on the action of the forces imparted by the propeller jet at the free surface are calculated as described here.

The acceleration is calculated using the velocities from the previous time step:

$$a_i = \frac{F_W}{M} \quad (3.10)$$

where a is the acceleration of the ice piece

F_W is the drag force acting on the ice floe

i is the time step number

M is the mass of the ice floe

$$F_W = 0.5\rho C_d V_{i-1}^2 \quad (3.11)$$

where ρ is the density of water

C_d is the drag coefficient

V_{i-1} is the velocity of the ice floe.

At each time step $t_i = t_{i-1} + \Delta t$, the velocity and position are then updated as given below:

$$V_i = V_{i-1} + a_i \Delta t \quad (3.12)$$

$$X_i = X_{i-1} + V_i \Delta t \quad (3.13)$$

where V is the velocity of the ice floe

X is the location of the ice floe

i is the time step number

Δt is the time step considered.

4 CHAPTER 4 - RESULTS

In this chapter, the predictions made by the model discussed and developed in the chapters 2 and 3 are presented. A C++ program was written to simulate the interaction of the propeller wake wash with pack ice and to predict the resulting change in concentration. The input to the simulation model is discussed, following which the predicted changes in concentrations when a pack ice field is subjected to propeller wake from the simulations are presented. The predictions from the simulations are compared with the experimental results carried out by Ferrieri (2012).

4.1 OVERVIEW OF THE SIMULATION METHOD

4.1.1 Experimental Work

The experimental work by Ferrieri (2012) studied the ability of a propeller to clear ice considering several factors. The influences of propeller shaft speed, initial ice concentration, inclination angle of the propeller, and distance from the propeller to the ice edge were studied. In order to ensure consistency between experiments, ice was modeled using pieces of polypropylene. Tracking software was used to record the movements of the ice pieces and to determine the changes in concentration. A 200 mm propeller outfitted to a podded propulsor was used for this experimental program. The podded propulsor unit was installed on the port side of a ship model. The ship model was installed transversely in a tow tank with the propeller wake wash flowing down the tank's length. The pod unit was operated in the tractor condition, in which the pod unit is behind the propeller during operation. Experiments were performed in a 4.0 m × 10.0 m pen created in the middle of the tank. The pen boundary was used to contain the ice

pieces during experimentation and was constructed using wire mesh. For each experiment, the propeller was run at the target shaft speed for 15 seconds.

4.1.2 Inputs to the model

Propeller shaft speed (n), diameter of the propeller (D_p), and thrust coefficient (K_t) are the primary inputs to be provided to the model for predicting the velocities at any point in the propeller jet. Based on the velocities predicted by the model, the motions of the ice floes can be calculated based on their characteristic properties and their downstream position with respect to the propeller. The inputs for the properties of the ice floes include density, dimensions and thickness. Based on the nature of the experiments, three more parameters were added to the model: initial concentration of the ice floes inside the penned areas, distance to the ice edge from the propeller, and inclination of the propeller. The required concentration of the ice floes were recorded from the video image of the ice field at the start time for each test case considered and were also provided to the model as input. Inputs to the model considered for the simulation based on the values used by Ferrieri (2012) are presented in Table 1 below.

Table 1. Model Inputs

D_p	0. 2 m
K_t	0.17
n	7.5, 10, 12.5
Ice floe Thickness	.0127 m
Ice floe density	900 kg/m^3
Distance to ice	0.4, 0.70, 1.0 m
Concentration	30%, 45%, 60%
Inclination angle	0^0, 2.5^0, 5^0

4.1.3 Ice Concentration Analysis

Four areas that spanned the ice pen were defined for carrying out the concentration analysis as shown in Figure 12 below. The start of Area 1 was positioned just beyond the turbulent region as the turbulence on the water's surface created additional glare which affected the concentration analysis. Ice floes tend to accumulate towards the end of the pen boundaries and hence the end boundary of Area 4 was not defined at the actual pen boundary but at a location which permitted ice to clear beyond Area 4. Appendix D contains the boundary definitions used in the ice analysis. The concentration time histories for specified areas in the ice field were analyzed for each test case considered. Custom software was used to calculate ice concentrations at various times from the video acquired during each test. Corresponding measurements of concentrations were made from the numerical model based on the parameters pertinent to each test case. The motion of ice floes in the model was restricted to prevent clearing beyond the lateral extend of the pen boundary.

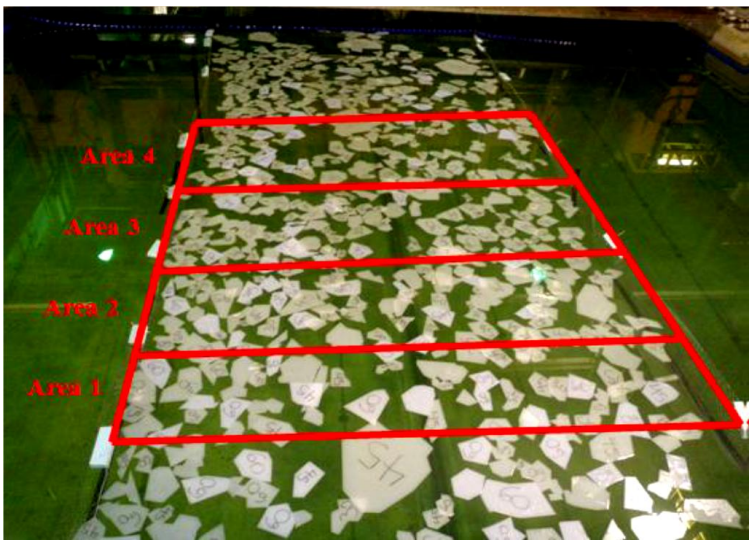

Figure 12. Example of analysis area (After Ferrieri, 2012)

4.2 RESULTS AND DISCUSSION

The concentration time history plots were made for the 11 test cases considered from the experimental results and were compared to the model predictions. For the comparison, the same initial concentration corresponding to the experiment was used for each area in a test case. The parameters varied during the experiment corresponding to each test case considered is given in Table 2 and was used in the model to predict the results for comparison. In the case of concentration, the value of concentration represents the average concentration of the whole pen area considered. The average concentration in Areas 1, 2, 3 and 4 varied and was calculated from image analysis at the start of the test case.

Table 2. Parameters for test cases

Test No.	Shaft Speed (RPS)	Incline Angle (Degree)	Distance to Ice edge (m)	Concentration
3	12.5	0	0.4	60%
1	12.5	0	0.4	30%
10	12.5	0	1	30%
4	12.5	5	0.4	60%
9	12.5	5	0.4	30%
2	12.5	5	1	30%
5	5	2.5	0.7	45%
12	10	-2.5	0.7	45%
11	10	2.5	0.1	45%
8	10	2.5	0.7	45%
6	10	2.5	0.7	45%

4.2.1 Time-Concentration History plots

The concentration time histories of the four areas for the test case 3 are plotted and explained below. Figures 13, 14, 15, and 16 show the comparison of the concentration over time between

the model prediction and the experimental results in Areas 1, 2, 3 and 4 for test case 3. The *X*-axis of the graphs represents the time starting from 0 seconds and ending at 15 seconds, which represents the end of the experiment. The *Y*- axis represents the concentration of ice floes. As shown, there are two lines on the plot: the experimental result is represented by the solid line and the dashed line represents the results predicted by the model. As the figures for the change in concentration for all 11 test cases can be interpreted in the same way, a representative case of test 3 is chosen and is explained. The time-concentration history figures for other test cases are given in the Appendix A.

The concentration at the beginning was at 66 % for both the model and experiment in case of Area 1. When the propeller was started and as the time progressed, the concentration in Area 1 showed a slight increase for both model and experimental results. This is due to the action of propeller wake and subsequent clearing of ice from regions upstream into Area 1. The concentration of ice floes in Area 1 increased initially for both model prediction and experiment from 66% to a maximum value of 70% at 2 seconds for the model prediction and a maximum value of 72% at 3 seconds for experimental results.

After the initial increase in concentration, the concentration decreased as the time progressed due to clearing of ice floes into Area 2, Area 3, Area 4 and farther downstream areas. After the decrease in the concentration, a stage was reached when the concentration was almost stagnant with time. For both experimental results and model predictions, the concentration became stagnant after 14 seconds. The final concentration predicted by the model was 20%. For experimental results, the final concentration was 18%, a difference of 2% compared to the

predicted ice concentration after 15 seconds. The time concentration history plot for Area 1 - Test case 3 is shown in Figure 13.

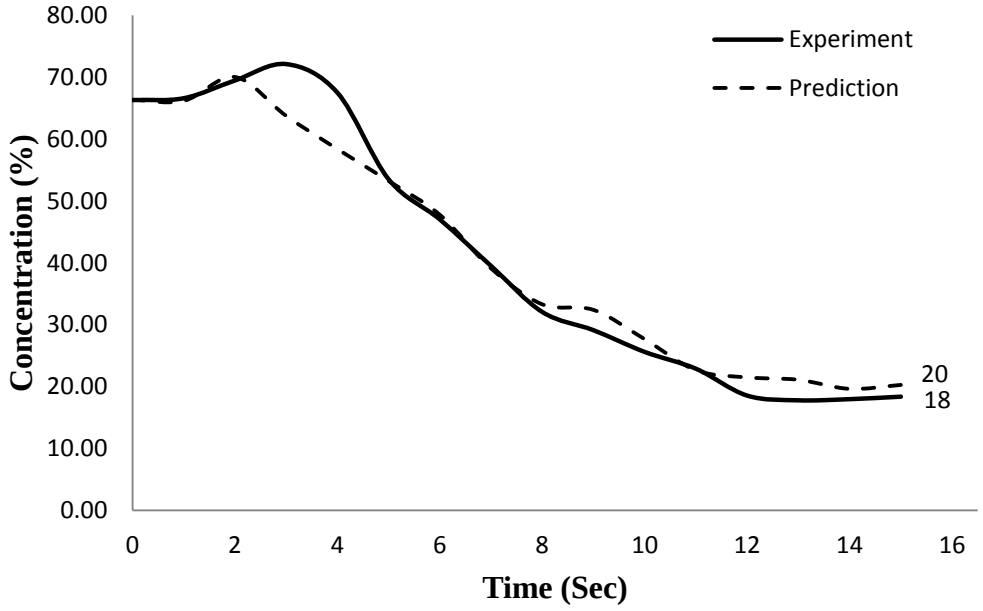

Figure 13. Time-concentration history plot for test 3 - Area 1

Considering Area 2 next, the concentration at the beginning was 59 % for both the model and experiment. The time concentration history plot for Area 2 is shown in Figure 14. When the propeller was started and the time progressed, the concentration in Area 2 increased for both the model and experimental results. This is due to the action of the propeller wake and subsequent clearing of ice from Area 1 and regions upstream into Area 2. The concentration of ice floes in Area 2 increases initially for both the model prediction and experiment from 59 % to a maximum value of 75 % at 5 seconds for model prediction and a maximum value of 71 % at 5 seconds for experimental results, after which it again started decreasing due to the clearing of ice floes into regions downstream of Area 2.

After the initial increase in concentration, the concentration decreases as the time advanced due to clearing of ice floes into Area 3, Area 4 and farther downstream areas. The final concentration predicted by the model is 18 % whereas for experimental results it is 23 %, showing a difference of 5 % for the ice concentration after 15 seconds.

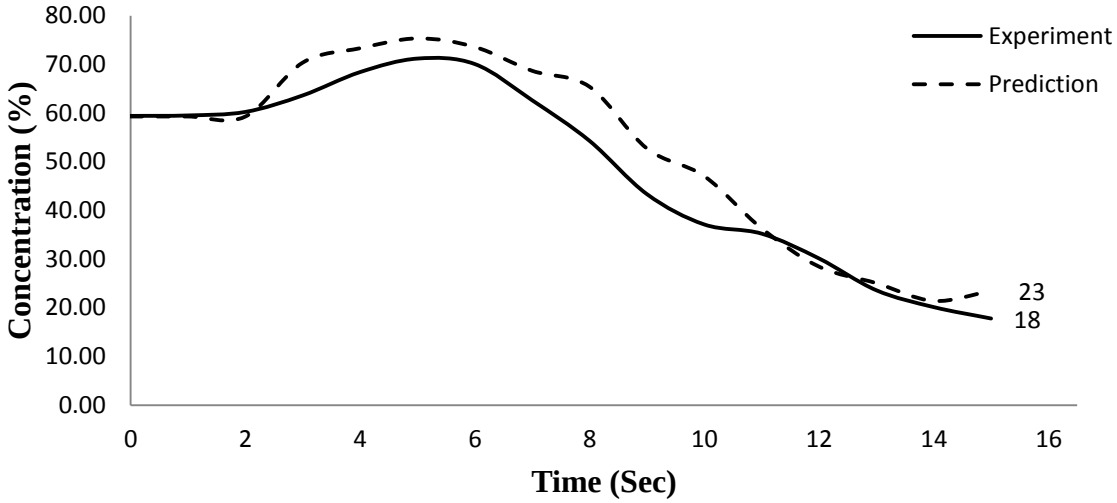

Figure 14. Time-concentration history plot for test 3 - Area 2

The same trend is seen for Area 3, as illustrated in Figure 15. The concentration at the beginning was maintained at 44 % for both the model and experiment. For both the model prediction and the experimental result, the concentration remained the same for up to 2 seconds, after which it gradually increased and reached a maximum value at 9 seconds. The maximum concentration was 68 % for the model prediction and 66 % for the experimental result. After 9 seconds, the concentration decreased till the end of the test at 15 seconds. The final concentration in the case of model predictions was 38% and for experimental results it was 30 %, showing a difference of 8 % after 15 seconds.

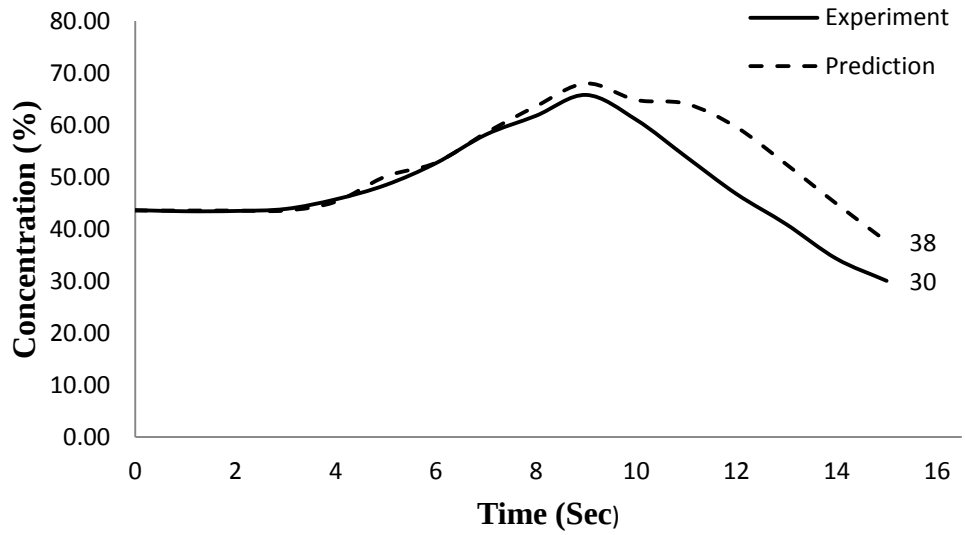

Figure 15. Time-concentration history plot for test 3 - Area 3

Figure 16 shows the comparison for Area 4 .The concentration at the beginning of time was kept at 41% for both the model and experiment. In the case of model prediction, the concentration remained the same for up to 7 seconds, after which it gradually increases and reaches the maximum value of 58 % at 15 seconds. For the experimental results, the concentration remains the same up to 7 seconds, then gradually increased until it reached its maximum value of 66% at 14 seconds and then decreased. The concentration over time showed similar trends in the case of both experimental and model predictions but experimental results shows a higher concentration of ice floes in Area 4 after 15 seconds when compared to model predictions due to faster clearing of ice floes into Area 4. The final concentration achieved in case of model predictions was 58 % whereas for experimental results it was 65 %, showing a difference of 7 % for the ice concentration at 15 seconds.

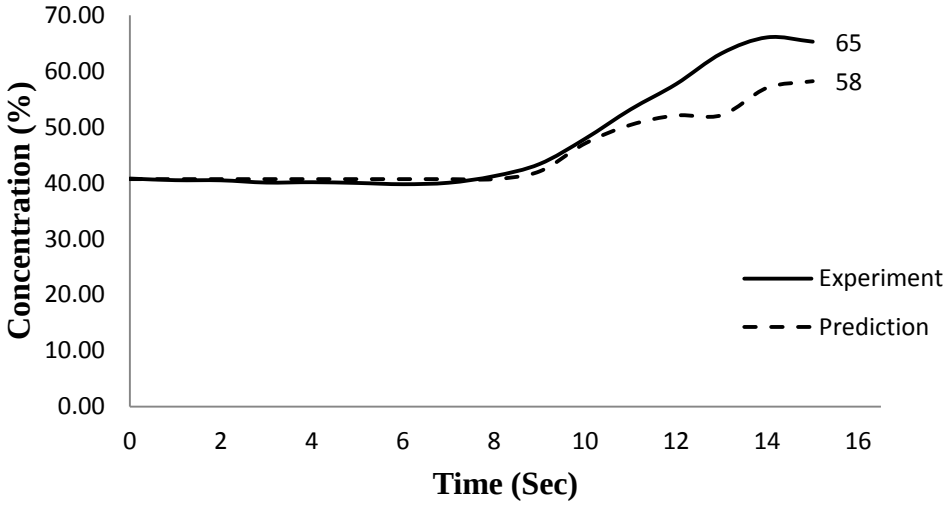

Figure 16. Time-concentration history plot for test 3 - Area 4

4.2.2 Final concentration

A clear understanding of the prediction capability of the model could be achieved by comparing the final concentrations in Areas 1, 2, 3 and 4 after 15 seconds. The final concentrations achieved after 15 seconds for both model predictions and experimental results for Areas 1, 2, 3 and 4 are summarized in Table 3. The difference in concentration after 15 seconds is also given in the Table. In all the test cases, ice floes were cleared away from Areas 1, 2 and 3 and got deposited into either Area 4 or areas farther downstream. Generally, at the end of 15 seconds we see a reduction in concentration in Areas 1, 2 and 3 and an increase in concentration in Area 4. The decrease in concentration in Areas 1, 2 and 3 was due to the clearing of the ice floes form these areas into Area 4 and farther regions due to the action of the propeller jet. Since the ice floes are getting cleared away, a negative value for the difference in concentration after 15 seconds

indicate that a lower amount of clearing was predicted by the model for Areas 1, 2 and 3 when compared to experimental results, whereas a positive value indicated a higher amount of clearing for the same areas. The increase in concentration in Area 4 was due to faster rate of deposition of ice floes when compared to ice floes getting cleared away into farther regions at the end of 15 seconds.

A comparison of the difference in concentrations observed after 15 seconds in Area 1 is discussed first. A lower clearing of ice floes was observed by the model for 3 test cases in case of higher shaft speed indicated by -2 %, -3% and -9% for the values of difference in concentration after 15 seconds for 12.5 RPS. In other cases of higher shaft speeds considered, the ice clearing predicted by the model was either 0% or slightly more by the values of 1%, 1% and 0%. At intermediate values of shaft speed i.e. for 10 RPS, the clearing predicted by the model was 0%, 2%, -1% and -3%. For the only test case with lower shaft speed i.e. 5 RPS, a lower value of ice clearing was predicted by the model indicated by -12%. Thus the difference in concentration varied from -12% to +2% in Area -1 giving an average value of -2% for the 11 test cases considered. Except for the 2 cases which show the higher variations i.e. -9% and -12%, the predictions made by the model in Area 1 shows good agreement with the experimental results. Thus it can be concluded that in Area 1 the prediction capability of the model agrees reasonably well with experimental results.

In Area 2 at a shaft speed of 12.5 RPS, a lower clearing is predicted by the prediction when compared to experimental results. In one case, the difference in concentration predicted by the model was significantly lower at -15%. In all other cases of higher shaft speeds also, the ice

clearing predicted by the model was also lower given by the values of -2%, -2%, -2%, -3% and -6%. At intermediate values of shaft speed i.e. for 10 RPS, a higher value of clearing was predicted by the model indicated by +2% and +2% for 2 test cases. At a shaft speed of 5 RPS, a prediction of lower ice clearing by the model was observed given by -2%. In Area 2, the prediction by the model varied from -15% to +2% giving an average value of -3% for the 11 test cases considered. Except for the high values of -6%, -10% and -15%, the predictions were near to the experimental results. However, a general trend of slightly lower clearing is observed for the predictions made by the model in Area 2.

The difference in concentration after 15 seconds for both the model prediction and experimental result in Area 3 is discussed here. A lower clearing of ice floes was predicted by the model for all the 6 test cases with higher shaft speed indicated by -6%, -8%, -8 %, -9%, -12% and -16% for the values of difference in concentration after 15 seconds. At intermediate values of shaft speed i.e. for 10 RPS, the clearing predicted by the model was also low giving -5%, -9% and -15% except for one test case with higher clearing of + 9%. For the only test case with lower shaft speed i.e. 5 RPS, a lower value of ice clearing of -15 % was predicted by the model. In case of Area 3, it varies from -16% to +9% giving an average value of -6% for the 11 test cases considered. The lower clearing observed for the predictions made by the model in Area 3 indicates that the ice floes have slowed down faster in the model.

In case of Area 4, the change in concentration after 15 seconds varies from 0% to +19% giving an average value of +5% for the 11 test cases. For 3 test cases with a shaft speeds of 12.5 RPS, ice floes which got cleared and deposited in Area 4 was higher for experimental results

indicated by values of +7%, +11% and +19%. In other cases with higher shaft speeds, the ice floes which got deposited in Area 4 was nearly equal to the experimental prediction indicated by 0%, 1% and 2%. At lower shaft speed of 5 RPS, no ice was cleared to Area 4 and hence there was no difference between the experimental results and the model predictions. For 2 cases with a shaft speed of 10 RPS, the predictions were similar and for the other 2 cases less ice was deposited by the model predictions indicated by +6% and +12%. From the lower value of deposition of ice floes in Area 4 predicted by the model, it can be concluded that the ice floes moved slower in the model.

Considering the turbulence in the flow, the predictions made by the model was closer to the experimental results for Areas 1, and 2. However, from comparison of the predictions in Areas 3, and 4 with the experimental results it can be concluded that the ice floes were moving slower in the model.

Table 3. Final concentration after 15 seconds

Run No.	Exp./Prediction	RPS	Incline Angle (Degree)	Dist to Ice edge (m)	Degree of Ice cover (%)	Area 1 (%)		Area 2 (%)		Area 3 (%)		Area 4 (%)	
							Δ		Δ		Δ		Δ
Run 3	Experiment Prediction	12.5	0	0.4	60%	18 20	-2	18 23	-6	30 38	-8	65 58	7
Run 1	Experiment Prediction	12.5	0	0.4	30%	2 11	-9	6 8	-2	17 25	-8	48 46	2
Run 10	Experiment Prediction	12.5	0	1	30%	5 5	0	4 5	-2	16 22	-6	37 36	1
Run 4	Experiment Prediction	12.5	5	0.4	60%	12 12	1	5 20	-15	24 33	-9	71 52	19
Run 9	Experiment Prediction	12.5	5	0.4	30%	3 6	-3	4 6	-2	5 17	-12	34 33	0
Run 2	Experiment Prediction	12.5	5	1	30%	9 7	1	6 10	-3	13 29	-16	48 37	11
Run 5	Experiment Prediction	5	2.5	0.7	45%	37 49	-12	54 56	-2	47 45	2	38 38	0
Run 12	Experiment Prediction	10	-2.5	0.7	45%	24 24	-1	41 39	2	60 75	-15	45 33	12
Run 11	Experiment Prediction	10	2.5	0.1	45%	18 21	-3	19 16	2	59 49	9	65 59	6
Run 8	Experiment Prediction	10	2.5	0.7	45%	18 16	2	18 28	-10	38 43	-5	43 43	0
Run 6	Experiment Prediction	10	2.5	0.7	45%	13 12	0	15 16	-1	32 41	-9	41 40	0

4.2.3 Comparison of model predictions at varying factors

The effect of three important factors on the results predicted by the model is discussed here. Model predictions were made using the model varying only one factor at a time and keeping other factors constant. The factors considered included shaft speed, inclination angle and distance to ice edge. The ice concentrations of test 3 was used and predictions made by varying shaft speed, inclination angle and distance to ice edge were recorded in Table 4, Table 5, and Table 6 below respectively.

The shaft speed was varied from 5 to 12.5 RPS and the results recorded are shown in Table 4 below. In Area 1, the concentration decreased from the initial concentration of 66% to final concentrations 48%, 22% and 20% after 15 seconds depending on the shaft speeds i.e. 5, 10 and 12.5 respectively. In Area 2, the concentration increases from 5% to 74% due to deposition of ice floes at 5 RPS. The concentration at 10 and 12.5 RPS decreases to 28% and 23% respectively. Area 1 and 2 shows increased capability of clearing away of ice floes with increases shaft speed. Similarly ice clearing capability of the model increased with increasing shaft speed in Areas 3, and 4. Thus the comparison of Area 1, 2, 3, and 4 shows increasing ice clearing capability with increasing shaft speed.

Table 4. Model prediction at different shaft speed

RPS	Time (s)	Area 1 (%)	Area 2 (%)	Area 3 (%)	Area 4 (%)
	0	66	59	44	41
5	15	48	74	53	41
10	15	22	28	60	52
12.5	15	20	23	38	58

The model prediction as the inclination angle of the propeller was varied from 0^0 to 5^0 is given in Table 5 below. As the propeller was directed towards the water surface by changing the inclination angle from 0^0 to 5^0, a corresponding decrease of ice floe concentration was found in Areas 1 and 3 due to clearing away of ice floes. . The concentration in Area 4 increases from initial concentration with increasing shaft speed due to deposition of ice floes. In Area 2, a clear trend was not observed. Thus from the results of Areas 1, 2, and 4 an increasing ice clearing capability is seen with small increase in inclination angle.

Table 5. Model prediction at different inclination angle at 12.5 RPS

Angle (Degree)	Time (s)	Area 1 (%)	Area 2 (%)	Area 3 (%)	Area 4 (%)
	0	66	59	44	41
0	15	20	23	38	58
2.5	15	19	24	33	59
5	15	18	24	34	60

The distance to ice was varied from 0.1 to 0.7 and the results are recorded in Table 6 below. A clear increasing or decreasing trend in ice floe concentration was not observed for Areas 1, and 2. In Area 3 it was seen that as the distance to ice edge was increased from 0.1 to 0.7, the final ice concentration achieved after 15 seconds increased from 30% to 47%, showing a decrease in ice clearing capability with increasing distance to ice edge. In Area 4, it was seen that less ice floes got deposited as the distance to ice edge was

increased from 0.1 to 0.7 m. Thus from the results of Areas 3, and 4, it was inferred that the ice clearing capability of the model decreases with increasing distance to ice edge.

Table 6. Model prediction at different distance to ice edge

Dist. To Ice Edge (m)	Time (s)	Area 1 (%)	Area 2 (%)	Area 3 (%)	Area 4 (%)
	0	66	59	44	41
0.1	15	21	21	30	59
0.4	15	20	23	38	58
0.7	15	19	22	47	55

5 CHAPTER 5 - DISCUSSION OF RESULTS AND CONCLUSION

5.1.1 Clearing of ice floes

The comparison of the model predictions with the experimental results showed that the predictions of ice clearing achieved in Areas 1 and 2 were better than for Areas 3 and 4, where the predicted ice clearing was slower. This is an indication that ice floes move slower in the model when compared to experimental ice floes. The reason behind the slower motion of the ice floes can be attributed to model discrepancies in the longitudinal decay of axial velocity, the lateral expansion of the surface current and the generation of waves due to the interaction of the jet with the free surface. The implications of these sources on the slower movement of ice floes are discussed below.

The longitudinal decay of axial velocity was modeled from experiment results of submerged propeller jets by previous researchers and hence the variation produced due to this component is limited to the changes in the geometric properties of the propeller. As the numerical model does not account for the detailed geometric properties of the propeller, there is room for improvement by developing a set of equations for this longitudinal decay for a number of propellers of different geometries. The potential improvement in the prediction power of the model due to this refinement is not expected to be significant.

The lateral expansion of surface current was modeled from the experimental measurements of Anthony (1990) for round jets by making an assumption of increased expansion for propellers. From the comparison of ice floes in Areas 1 and 2, it was seen

that a close match was obtained between the model prediction and experimental results. Thus it can inferred that the lateral clearing obtained by using this assumption is satisfactory and the lesser clearing observed in Areas 3 and 4 is due to the slower longitudinal movement of the ice floes. Even though this assumption would not result in slower longitudinal motion of ice floes, it should be validated by carrying out experiments to study the generation of surface currents by propellers.

A significant contribution to the slower movement of ice floes is assumed to come from the modeling of the effects of waves. The modeling of waves was limited to modifications in the tangential component of velocity and no change was made to the axial component of velocity. Even though previous experiments were carried out to study the generation of waves by submerged jets, the recorded data was not sufficient to model this effect accurately. It was observed from the experimental videos recorded by Ferrieri (2012) that momentum is imparted to the ice floes by the generated waves and a significant contribution to the ice floe motion comes from the effect of these waves. By studying and modelling the effect of these generated waves, a significant improvement is expected in the axial component of velocity. Such an improvement might address the predictions of slower motion of ice floes and thus ice clearing achieved by the model in Areas 3 and 4 can be improved.

5.1.2 Comparison of model prediction with experimental results

The experiment carried out by Ferrieri (2012) was aimed at finding the significant factors associated with ice floe clearing by a propeller jet. The factors considered included shaft

speed, inclination angle and distance to ice edge. The effect of these factors observed in the results predicted by the model and the corresponding results obtained during the experiments is discussed here. The experimental results supported the model predictions for both shaft speeds and inclination angle of the propeller. The model prediction with different distance to ice edge contradicted the experimental results.

A higher clearing of ice floes was observed at high shaft speed for both model predictions and experimental results and a lower shaft speed resulted in a lower clearing. An explanation of this observation could be that at lower shaft speeds less energy is imparted to the ice floes by the jet, which will in turn make the floes travel at slower speeds. As a result, observed clearing was also lower at lower shaft speeds. At higher shaft speeds, higher energy was imparted to the ice floes by the jet and correspondingly the amount of clearing observed was also higher.

A higher clearing was also observed for both model predictions and experimental results when the inclination angle of the propeller was increased. By changing the inclination angle of the propeller, the propeller jet is directed more towards (or away from) the water surface. By directing the jet towards the surface, a higher velocity of water acts at the surface and hence higher momentum is imparted to the ice floes near the surface resulting in more ice clearing.

From the analysis of experimental results, it was indicated by Ferrieri (2012) that the distance between the propeller and ice edge was not a significant factor. In the model, higher clearing was observed as the propeller was moved towards the ice edge and lower

clearing was observed as the propeller moved away from the ice edge. From a practical view point, the distance between the propeller and ice edge should influence the clearing of the ice floes. It may be inferred that the turbulence in the propeller jet might have played a confounding role in the experimental results, which was absent in the model predictions.

Bibliography

Anderson, K.G., McDonald, D., Mitten, P., Nicholls, S., Tait, D. 1986. Management of Small Ice Masses. *Environmental Studies Revolving Funds,* Report No. 042.

Anthony, D. G. 1990. The Influence of a Free Surface on the Development of Turbulence in a Submerged Jet. *Ph.D. Thesis*. The University of Michigan.

Albertson, M. L., Dai, Y. B., Jensen, R. A., and Rouse, H. 1950. Diffusion of a submerged jet. Transcript of the ASCE, Vol. 115, No. 409, 639-669.

Blaauw, H.G., Van de Kaa, E.J. 1978. Erosion of bottom and sloping banks caused by the screw race of manoeuvring ships. Delft Hydraulics Laboratory, Netherlands. 202.

Brewster, P. M. 1997. Modelling the wash from a ship's propeller, *Ph.D Thesis*, Queen's University of Belfast, UK.

Barker, A., Timco, G., Sayed, M., Wright, B. 2000. Numerical simulation of the "Kulluk" in pack ice conditions. *Proceedings, International Symposium on Ice*. Volume1, 165-171. Gdansk.

Comfort, G., Singh, S., Spencer, D. 2001. Moored vessel station-keeping in ice-infested waters: An assessment of model test data for various structures and ship shapes. *Proceedings, Port and Ocean Engineering under Arctic Conditions,* Ottawa.

Crocker, G., Wright, B., Thistle, S., Bruneau, S. 1998. An assessment of current iceberg management capabilities. Report for: National Research Council Canada, Prepared by C-Core and B. Wright & Associates, Ltd.. *Program of Energy Research and Development/ CHC Report 20-33.*

Edmond, C., Liferov, P., Metge, M. 2011. Ice and iceberg management plans for Shtokman field. *Proceedings, Offshore Technology Conference,* Houston.

Eik, K. 2008. Review of experiences within ice and iceberg management. *The Journal of Navigation, 61:* 557-572.

Eik, K., Gudmestad, O.T. 2010. Iceberg management and impact on design of offshore structures. *Cold Regions Science and Technology 63:*15–28.

Ferrieri, J.M. 2012. Experimental Study on Ice Management through the use of Podded Propeller Wash 2012. *Master's Thesis*. Memorial University of Newfoundland.

Fuehrer, M., Romisch, K. 1977. Effects of modern ship traffic on islands and ocean waterways and their structures.*Proceedings 24th Congress P.I.A.N.C.,* Leningrad, Sections1–3.

Hamill, G. A. 1987. Characteristics of the screw wash of a manoeuvring ship and the resulting bed scour. *PhD Thesis*. Queen's University of Belfast, UK.

Hamill, G.A., McGarvey, J.A., Hughes, D.A.B. 2004. Determination of the efflux velocity from a ship's propeller. *Proceedings of the Institution of Civil Engineers: Maritime Engineering*, 157 (2), 83–91.

Hashmi, H. N. 1993. Erosion of a granular bed at a quay wall by a ship's screw wash. *PhD Thesis*. Queen's University of Belfast, UK.

Hamilton, J.M. 2011. The challenges of deep water arctic development. *Proceedings, International Offshore and Polar Engineering Conference*, Hawaii.

Hinkel, A.M., Thibodeau, S.L., Hippman, A. 1988. Experience with drillship operations in the u.s. beaufort sea. *Proceedings, Annual Offshore Technology Conference*, Houston.

International Organization for Standardization. (2010). International Standard: Petroleum and Natural Gas Industries – Arctic Offshore Structures. ISO/FDIS 19906:2010(E).

Keinonen, A. J. 2008. Ice management for ice offshore operations. *Proceedings, Offshore Technology Conference*, Houston.

Keinonen, A.J., Lohi, P. 2000. Azimuth and multipurpose icebreaker technology for arctic and non-arctic offshore. *Proceedings, Offshore and Polar Engineering Conference*, Seattle.

Keinonen, A. J., Browne, R., Lam, E., Jolles, W. 2006 a. Six years in Sakhalin offshore oil – management of risk, operations in ice. *Proceedings, International Conference on Port and Ocean Engineering under Arctic Conditions.*

Keinonen, A. J., Shirley, M., Liljeström, G., Pilkington, R. 2006 b. Transit and stationary coring operations in the central polar pack. *Proceedings, International Conference on Port and Ocean Engineering under Arctic Conditions.*

Johansson, P., George, W. 2006. The far downstream evolution of high-Reynoldsnumber axisymmetric wake behind a disk, part 1: Single point statistics. *Journal of Fluid Mechanics, 555,* 363-385.

Lee, J.H.W., Chu, V.H. 2003. Turbulent Jets and Plumes, A Lagrangian Approach. *Kluwer Academic Publishers. ISBN: 1-4020-7520-0.*

Loberto, A. 2007. An experimental study on the mixing performance of boat propellers. *Ph.D. Thesis* .The Queen's University of Belfast.

Lam, W. H., Hamill, G. A., Robinson, D., Raghunathan, S. 2010. Observations of the initial 3D flow from a ship's propeller. *Journal of Ocean Engineering, 37,* 1380-1388.

Lam, W. H., Song, Y., Raghunathan, S., Hamill, G. A., Robinson, D. 2011a. Investigation of a ship's propeller jet using momentum decay and energy decay. *Canadian Journal of Civil Engineering, 38.*

Lam, W.H., Hamil, G.A., Song, Y.C. 2011b. Experimental investigation of the decay from a ship's propeller. *China Ocean Engineering, 25:2*, 265-284.

Lam, W.H., Hamil, G.A., Song, Y.C., Robinson, D.J., Raghunathan, S. 2011c. A review of the equations used to predict the velocity distribution within a ship's propeller jet. *Journal of Ocean Engineering, 38, 1-10.*

Lam, W.H., Hamil, G.A., Raghunathan, S., Song, Y.C. 2012. Analysis of the 3D zone of flow establishment from a ships propeller. *KSCE Journal of Civil Engineering 16(4):465-477.*

Maddock, B., Bush, A., Wojahn, T., Kokkinis, T., Younan, A., Hawkins, J.R. 2011. Advances in ice management for deepwater drilling in the Beaufort Sea. *Proceedings, International Conference on Port and Ocean Engineering under Arctic Conditions,* Montréal.

Madnia, K., Bernal, L.P. 1989. Interaction of a turbulent round jet with the free surface. Department of Aerospace Engineering, THE UNIVERSITY OF MICHIGAN. Technical Report No. 89-05l

Montgomery, D. 2009. Design and Analysis of Experiments (Eighth Edition). *John Wiley & Sons, Inc.*

McGarvey, J. A. 1996. The influence of the rudder on the hydrodynamics and the resulting bed scour, of a ship's screw wash, *PhD Thesis*. Queen's University of Belfast, UK.

Prosser, M. 1986. Propeller induced scour. Tech. Rep., BHRA Project RP A01415, The Fluid Engineering Centre, Cranfield.

Pilkington, G.R., Wright, B.D., Dixit, B.C., Woolner, K.S., O'Dell, B.D. 1988. A review of Kulluk's performance after three years operations in The Beaufort Sea.

Pilkington, R., Keinonen, A.J, Sheikin, I.B. 2006. Ice observations and forecasting during the arctic coring project, August - September 2004. *Proceedings, International Conference And Exhibition on Performance of Ships and Structures in Ice.*

Sayed, M., Barker, A. 2011. Numerical Simulations of ice interaction with a moored structure. *Proceedings, Arctic Technology Conference*, Houston.

Situ, R., Brown, R., Loberto, A. (2010). Experimental stud of the concentration field of discharge from a boat propeller. *Environmental Fluid Mechanics, 10*, 657-675.

Spencer, D., Molyneux, W.D. 2009. Predicting pack ice loads on moored vessels. *Proceedings, International Conference on Ship & Offshore Technology*, Busan.

Stewart, D. P. J. 1992. Characteristics of a ships screw wash and the influence of quay wall proximity. *PhD Thesis*. Queen's University of Belfast, UK.

Wright, B. 1998. Moored vessel stationkeeping in Grand Banks pack ice conditions. Report for: National Research Council Canada, Prepared by B. Wright & Associates Ltd., Canatec Consultants Ltd. and AKAC Inc.. *Program of Energy Research and Development/ CHC Report 26-189.*

Wright, B. 1999. Evaluation of full scale data for moored vessel stationkeeping in pack ice. Report for: National Research Council Canada, Prepared B. Wright & Associates Ltd.. *Program of Energy Research and Development/ CHC Report 26-200.*

Wright, B. 2000. Full scale experience with Kulluk stationkeeping operations in pack ice (With reference to Grand Banks developments). Report for: National Research Council Canada, Prepared by B. Wright & Associates Ltd.. *Program of Energy Research and Development/ CHC Report 25-44.*

Wright, B. 2001. Ice loads on the Kulluk in managed ice conditions. *Proceedings, International Conference on Port and Ocean Engineering under Arctic Conditions*, Ottawa.

Wygnanski, I., Fiedler, H. 1969. Some Measurements in the Self-Preserving Jet. *Journal of Fluid Mechanics, 38 (3), 577-612.*

Zhou, L., Su, B., Riska, K., Moan, T. 2011. Numerical simulation of moored structure station keeping in level ice. *Cold Regions Science and Technology.*

Appendix - A

Time-concentration history plots for Areas 1, 2, 3, and 4 for Tests 1 to Test 12.

Time-concentration history plot for test 1 - Area 1

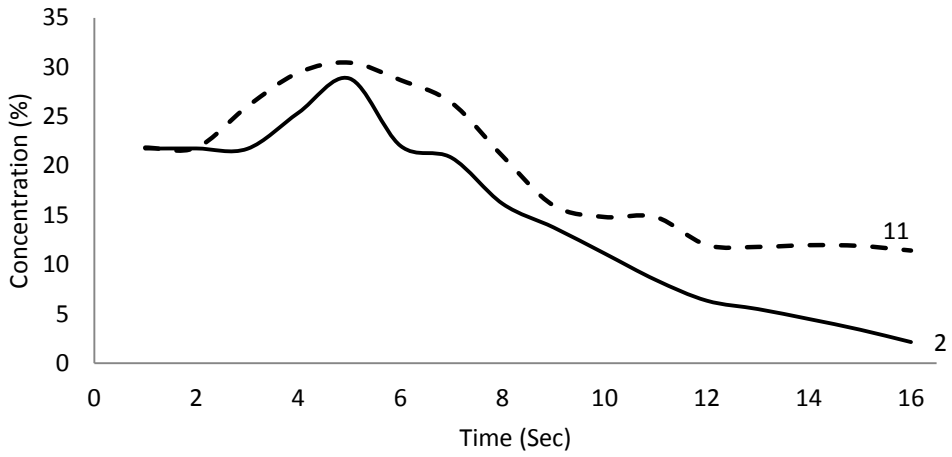

Time-concentration history plot for test 1 - Area 2

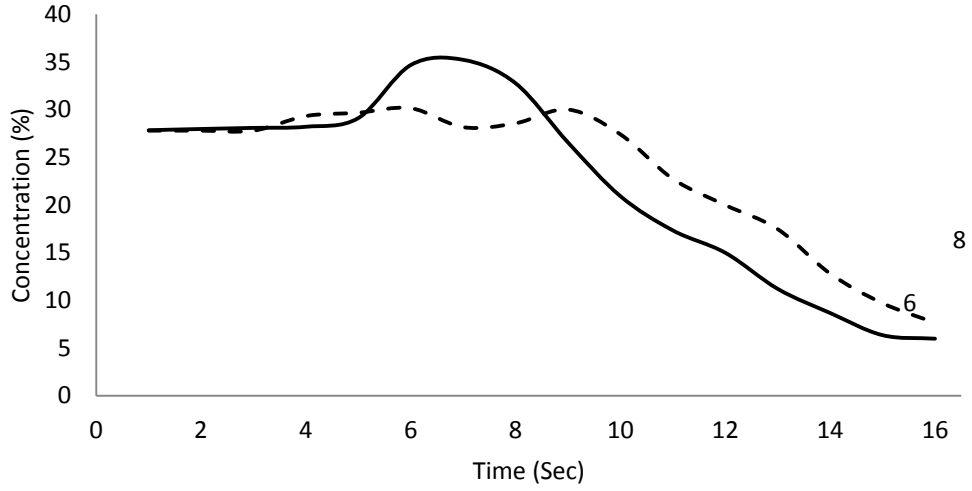

Time-concentration history plot for test 1 - Area 3

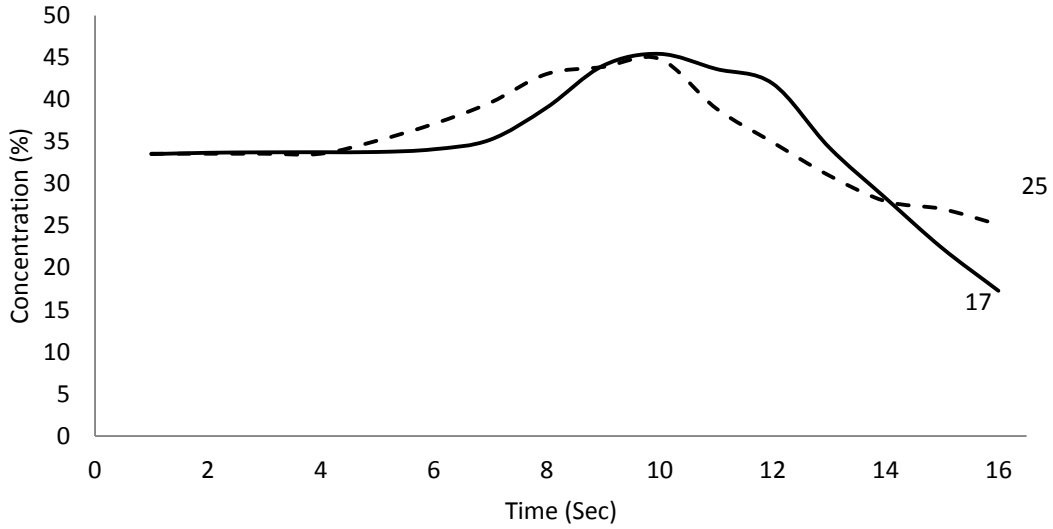

Time-concentration history plot for test 1 - Area 4

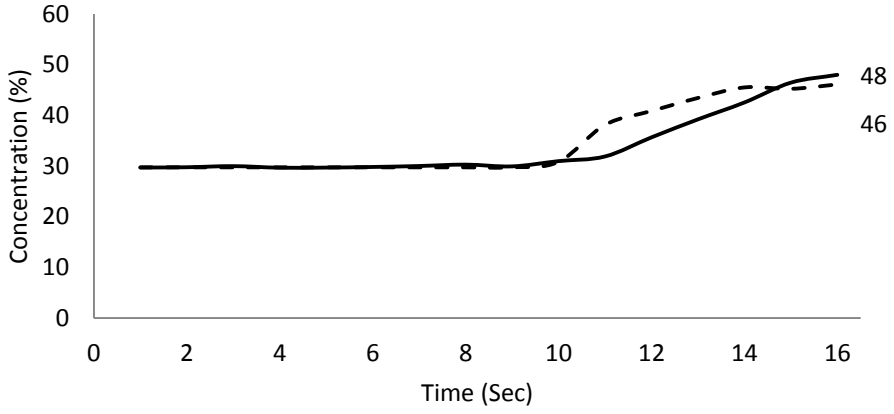

Time-concentration history plot for test 2 - Area 1

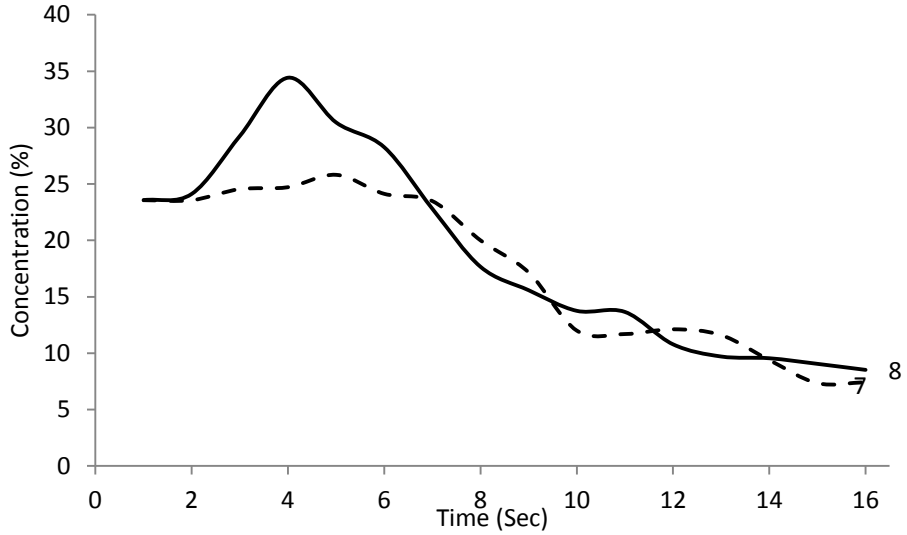

Time-concentration history plot for test 2 - Area 2

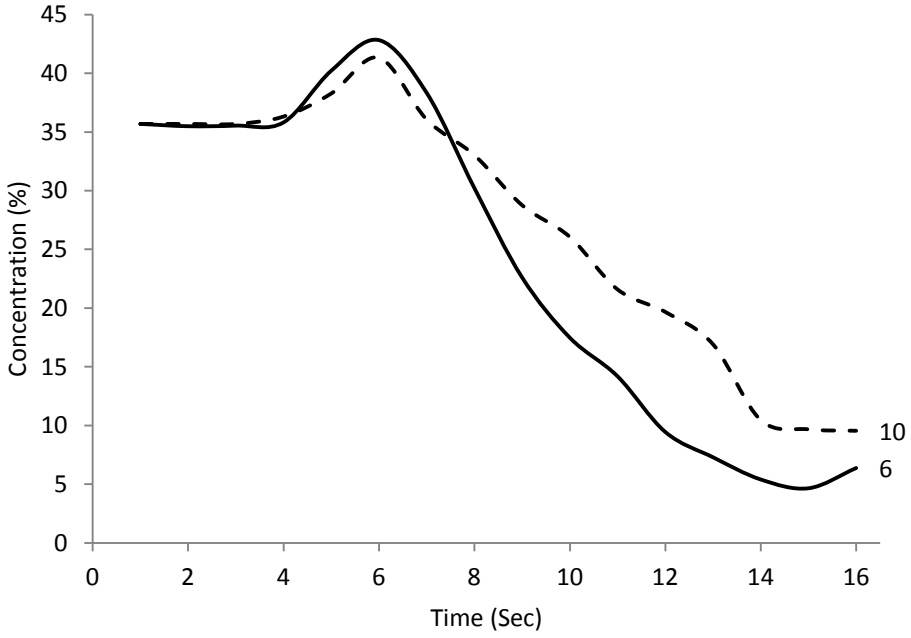

Time-concentration history plot for test 2- Area 3

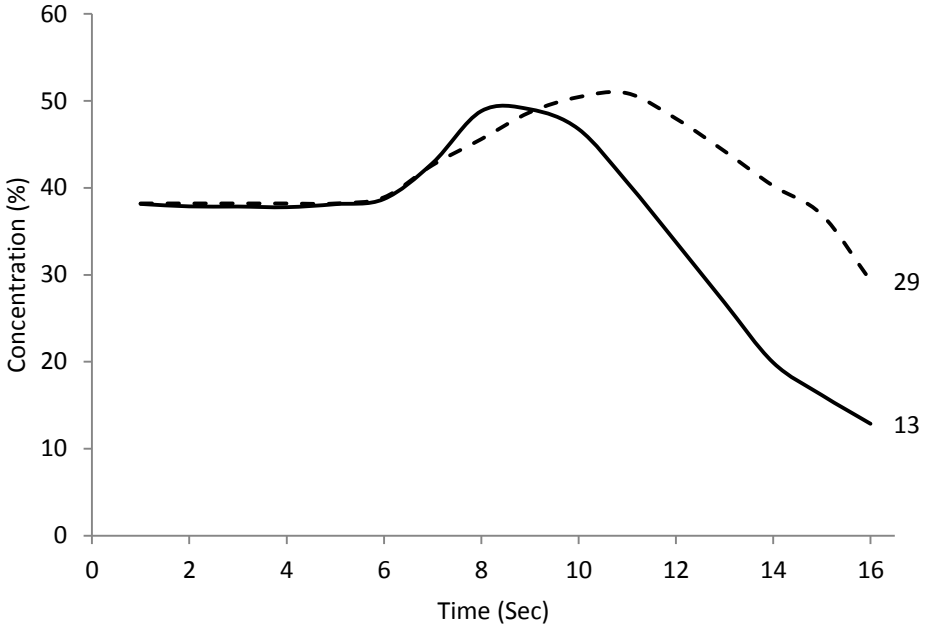

Time-concentration history plot for test 2 - Area 4

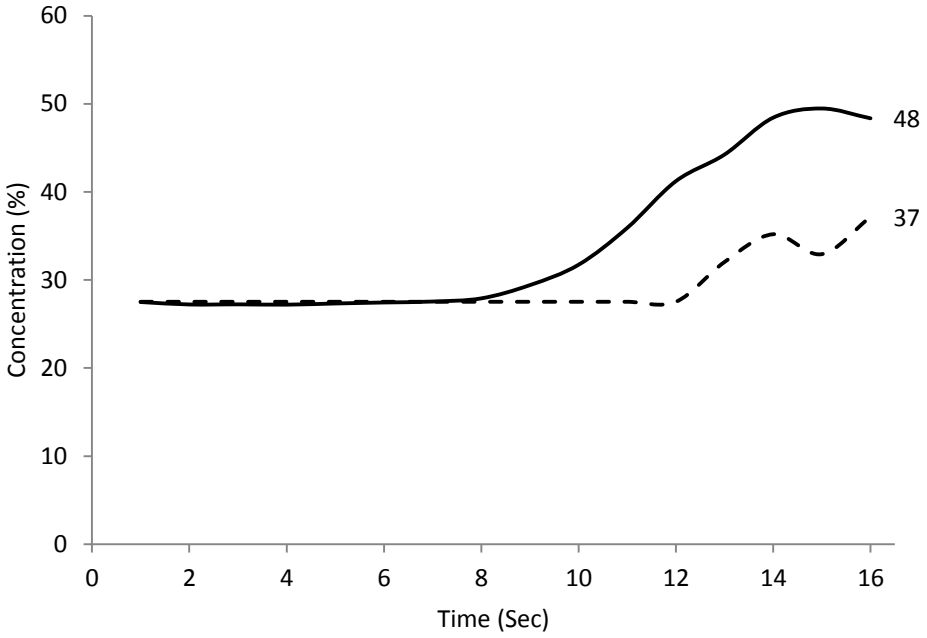

Time-concentration history plot for test 4 - Area 1

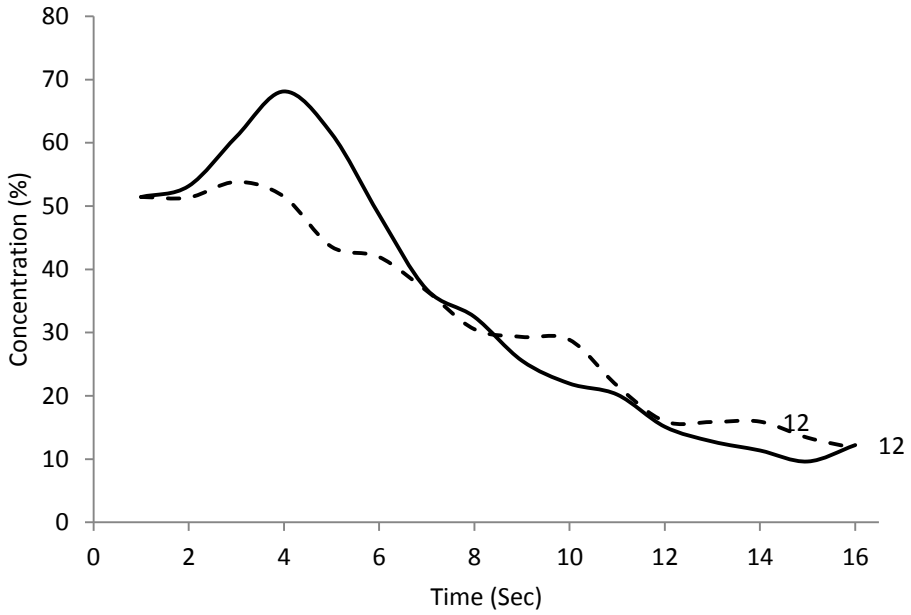

Time-concentration history plot for test 4- Area 2

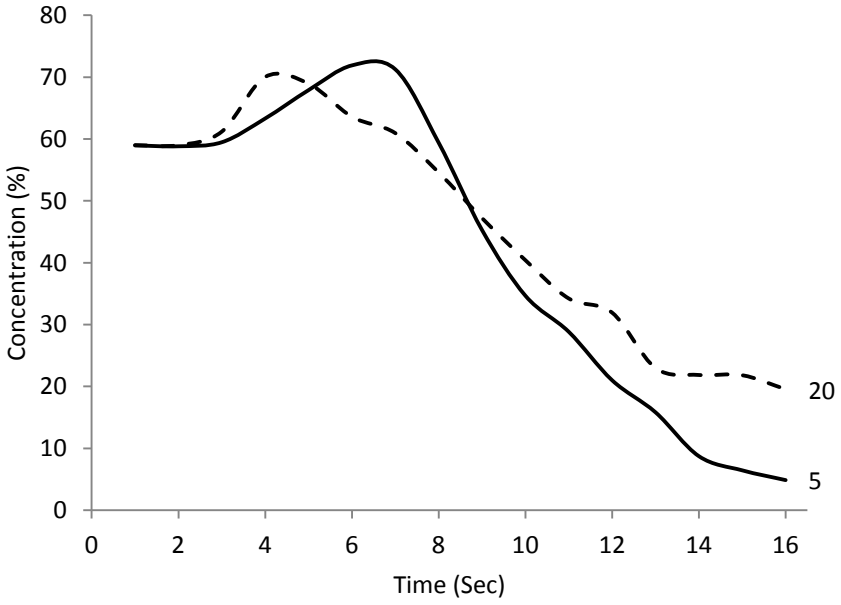

Time-concentration history plot for test 4- Area 3

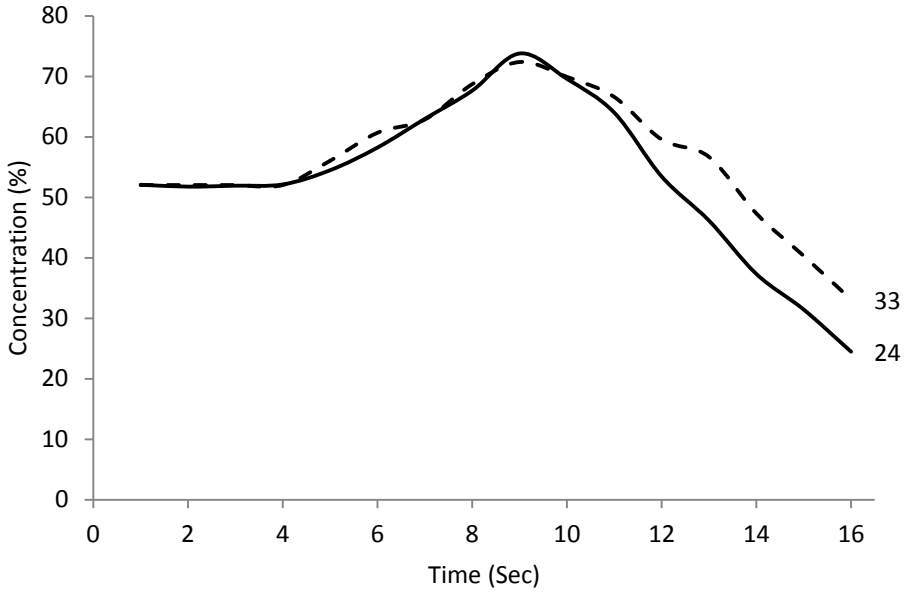

Time-concentration history plot for test 4 - Area 4

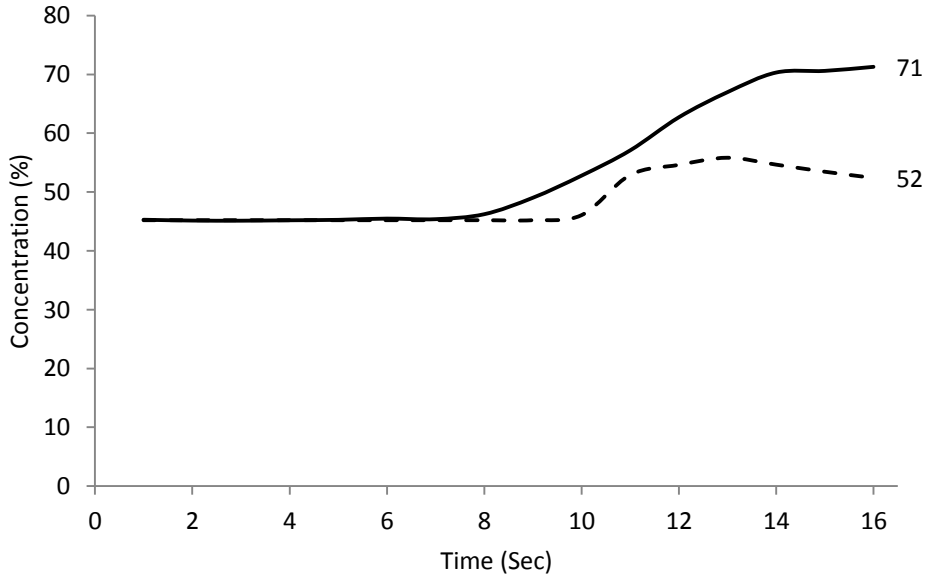

Time-concentration history plot for test 5 - Area 1

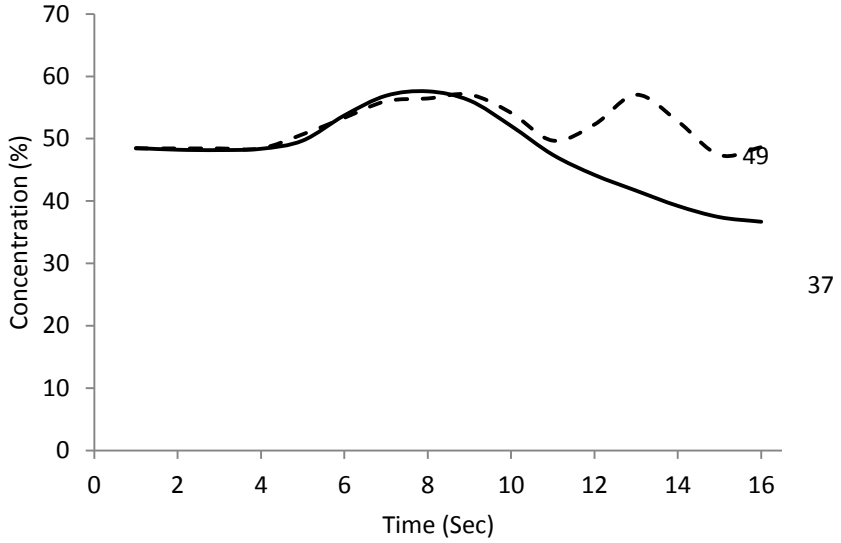

Time-concentration history plot for test 5 - Area 2

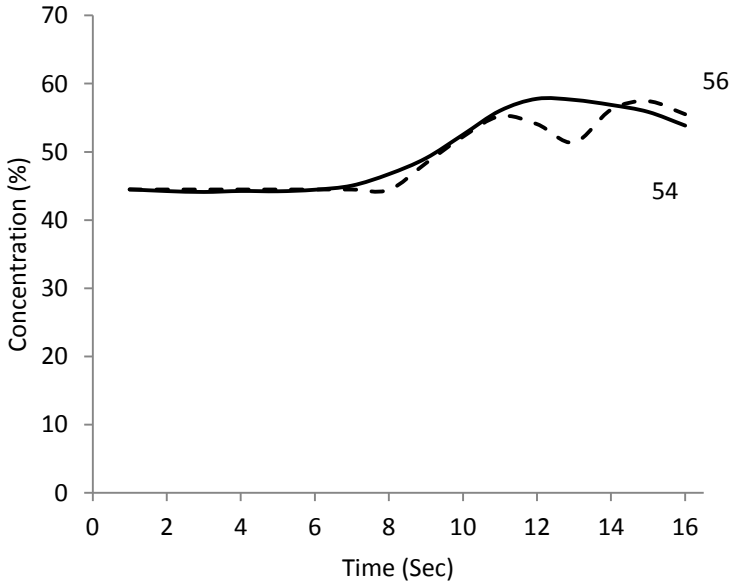

Time-concentration history plot for test 5- Area 3

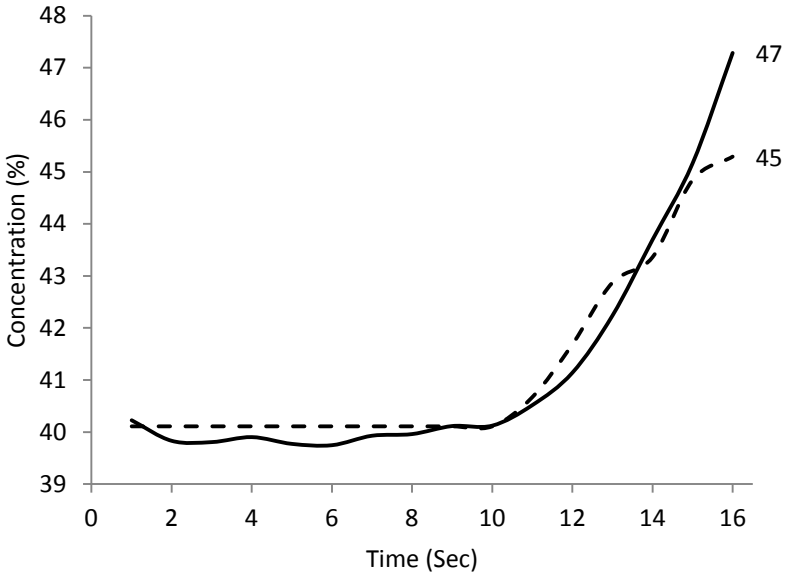

Time-concentration history plot for test 5 - Area 4

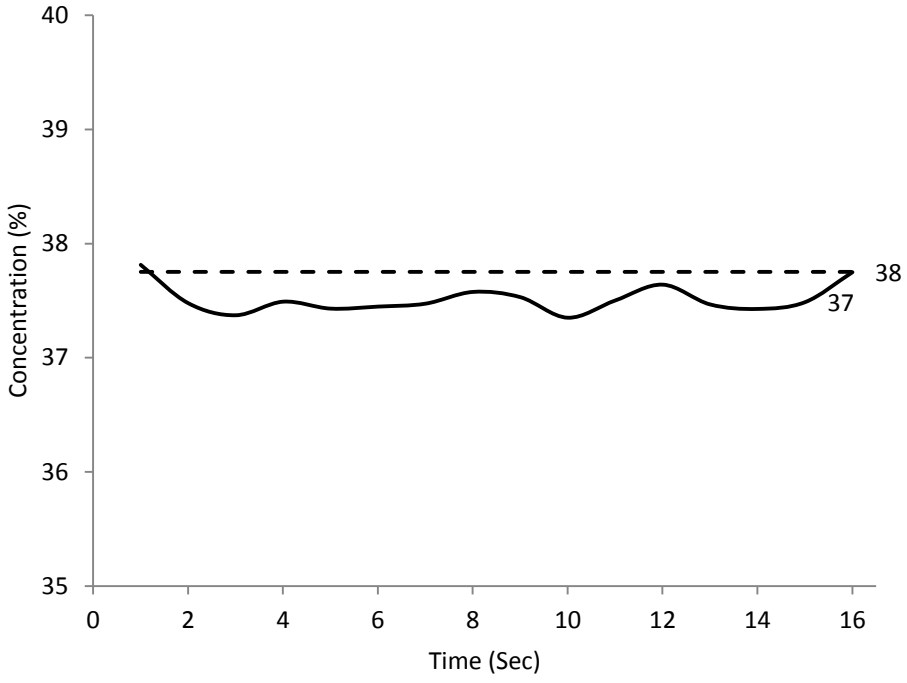

Time-concentration history plot for test 6 - Area 1

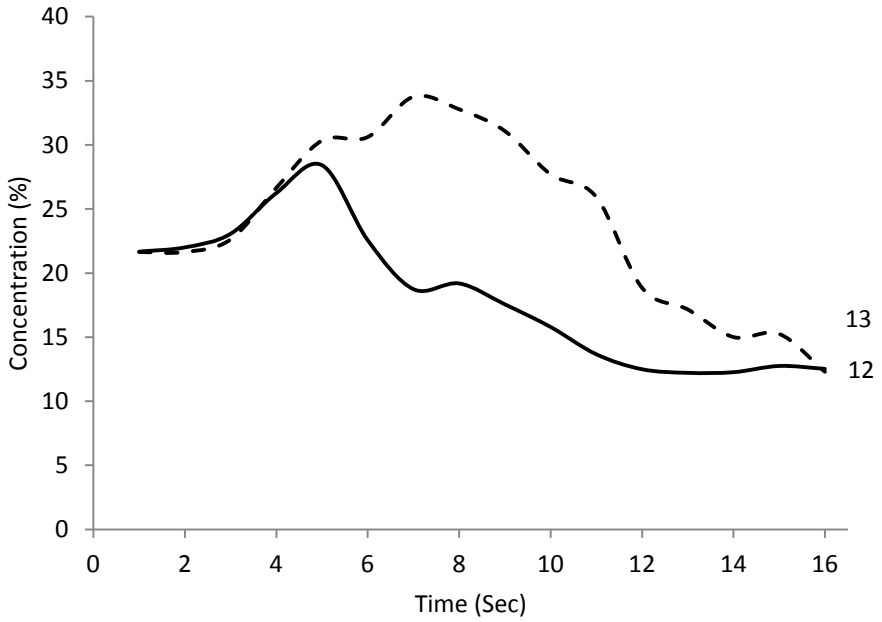

Time-concentration history plot for test 6 - Area 2

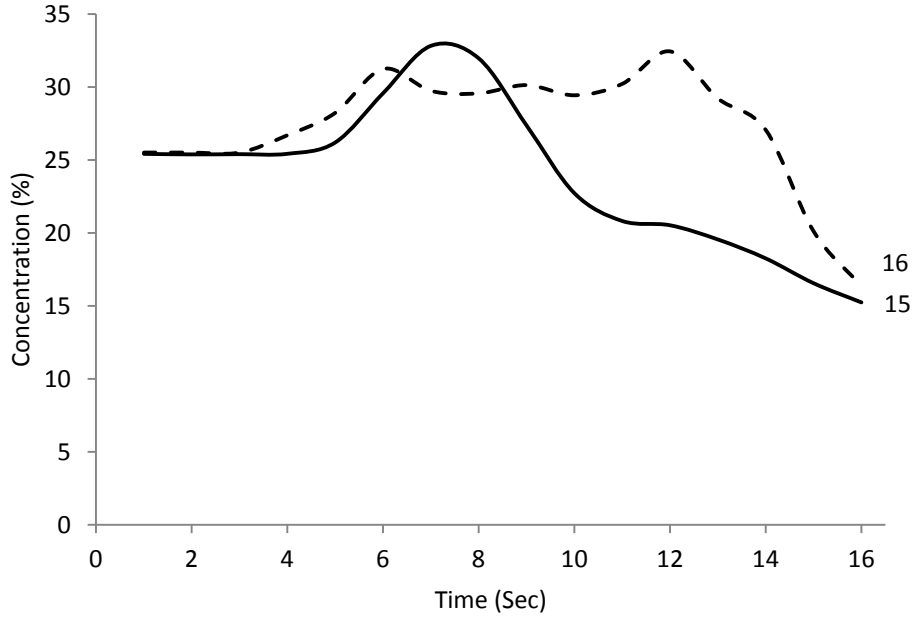

Time-concentration history plot for test 6- Area 3

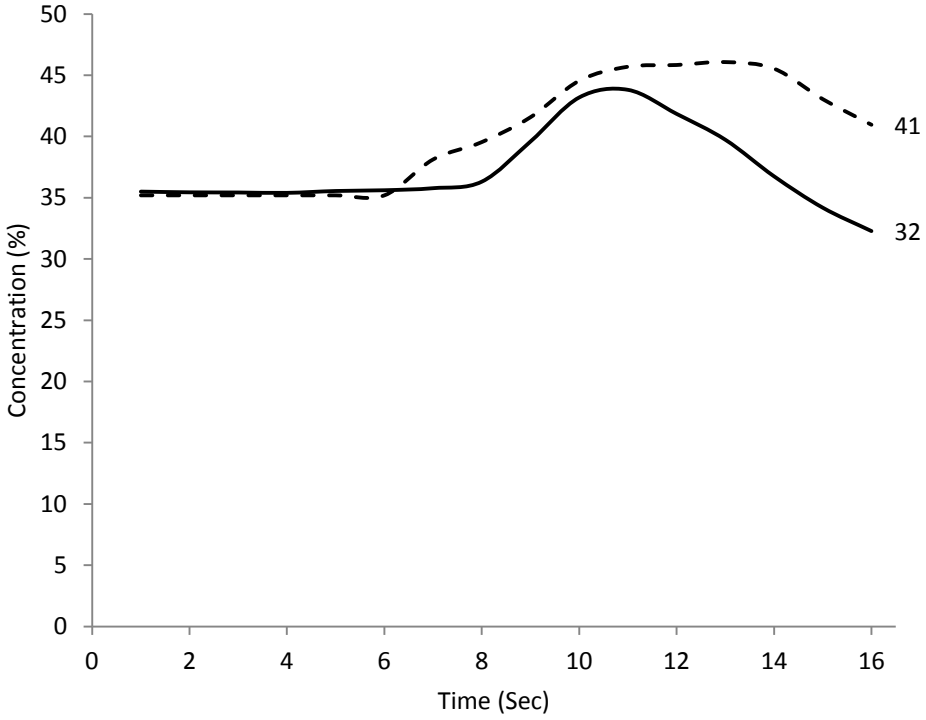

Time-concentration history plot for test 6 - Area 4

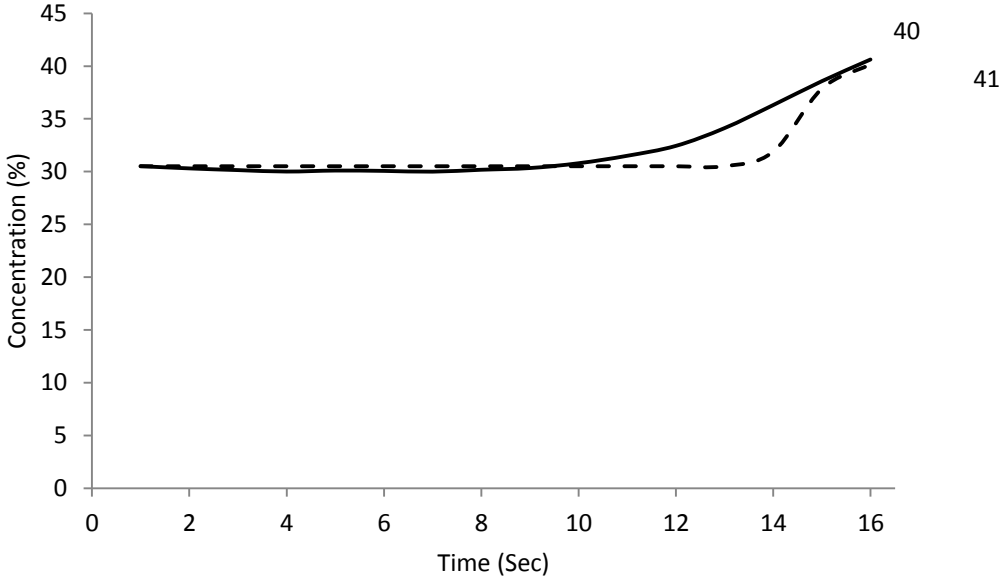

Time-concentration history plot for test 8 - Area 1

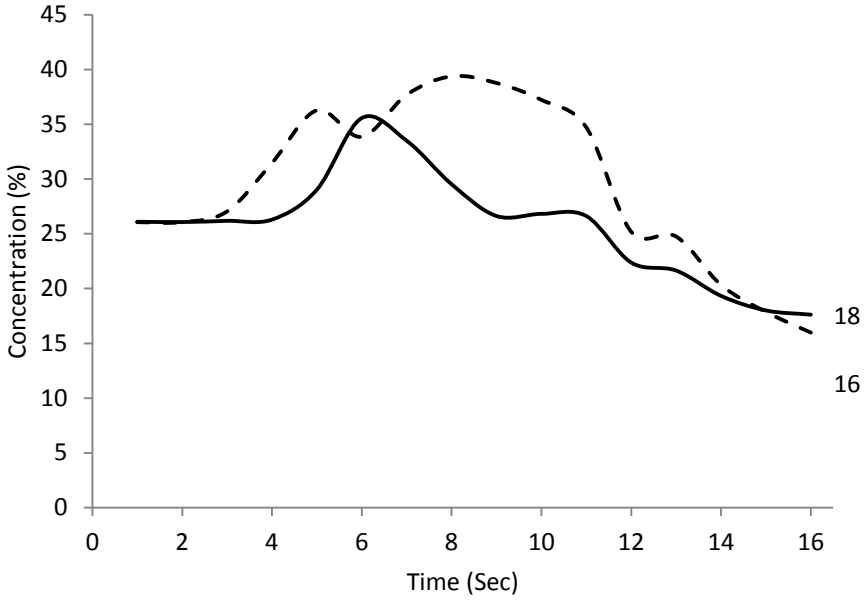

Time-concentration history plot for test 8 - Area 2

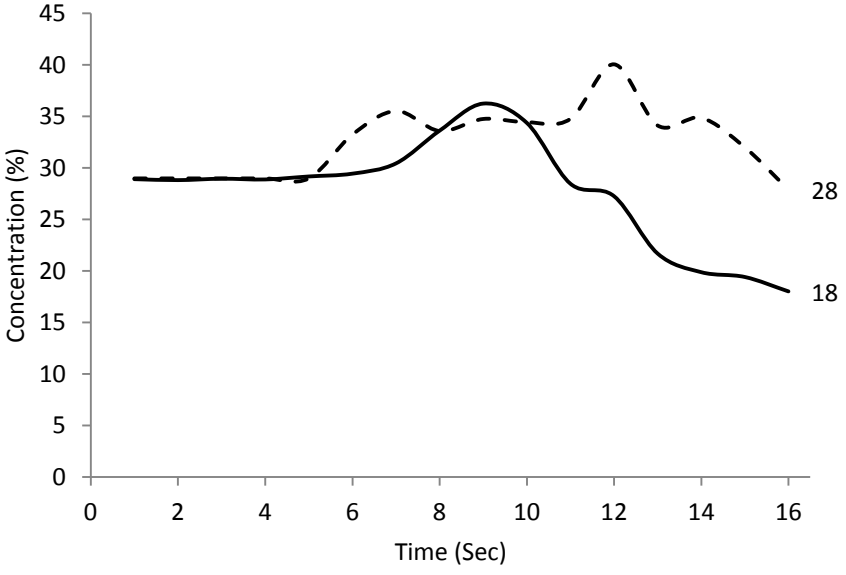

Time-concentration history plot for test 8- Area 3

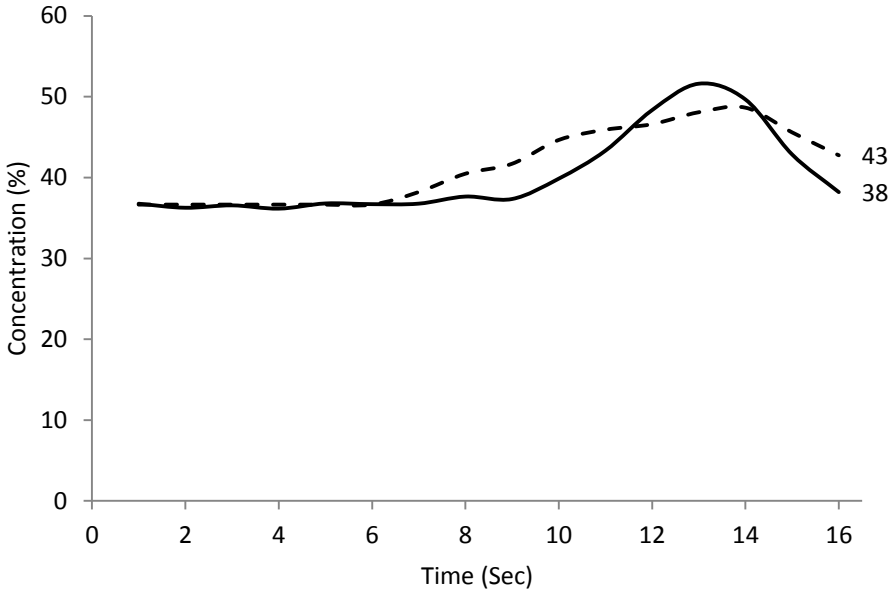

Time-concentration history plot for test 8 - Area 4

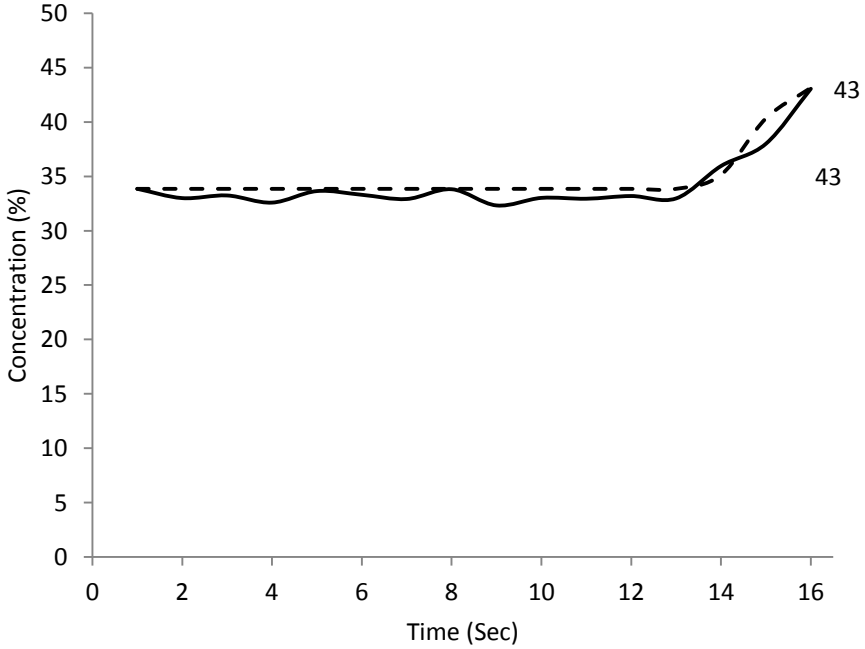

Time-concentration history plot for test 9 - Area 1

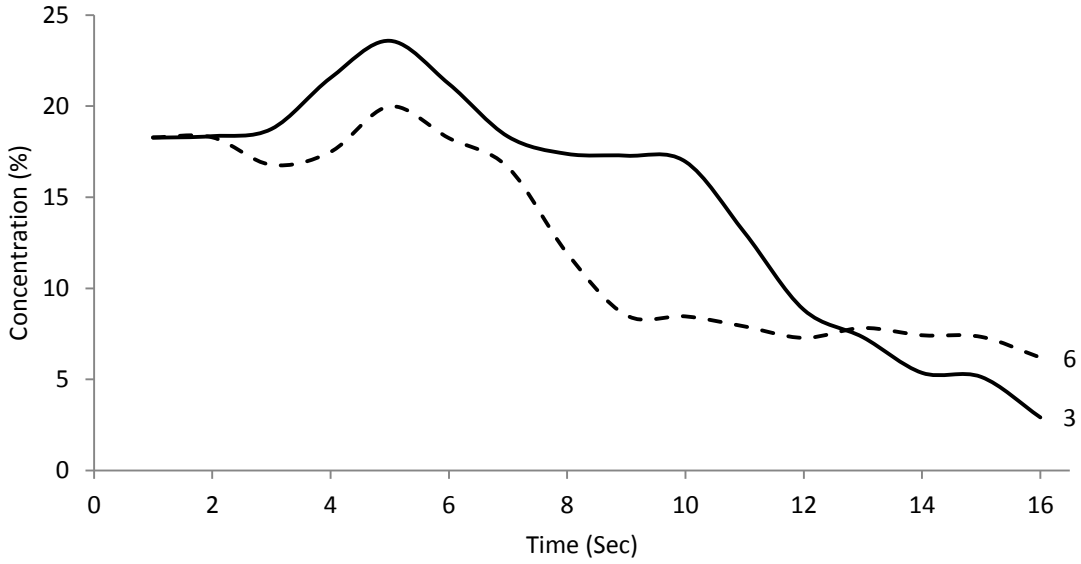

Time-concentration history plot for test 9 - Area 2

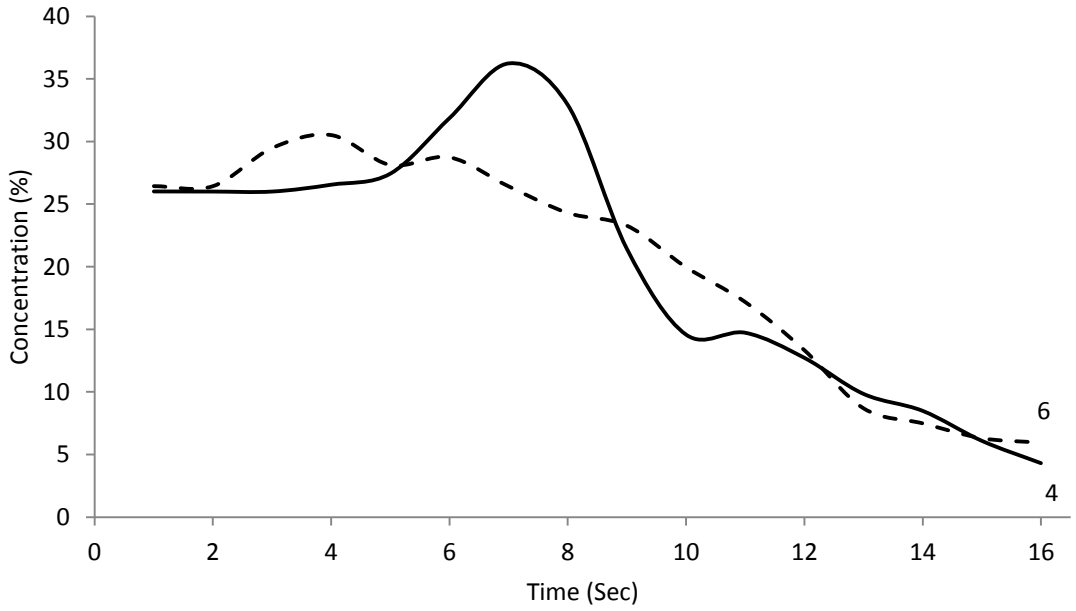

Time-concentration history plot for test 9- Area 3

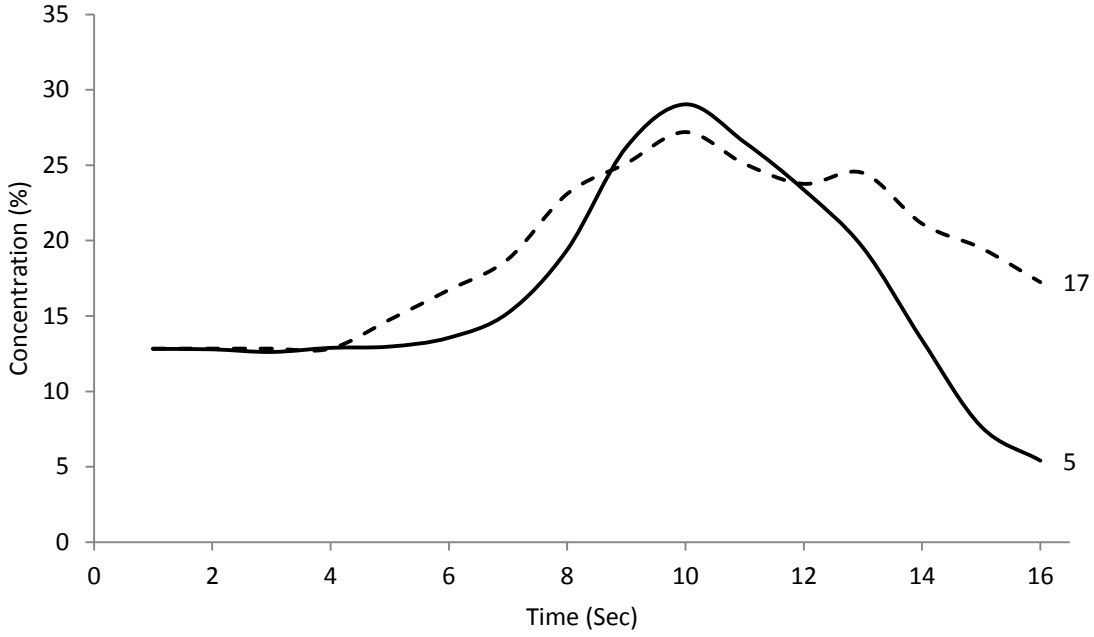

Time-concentration history plot for test 9 - Area 4

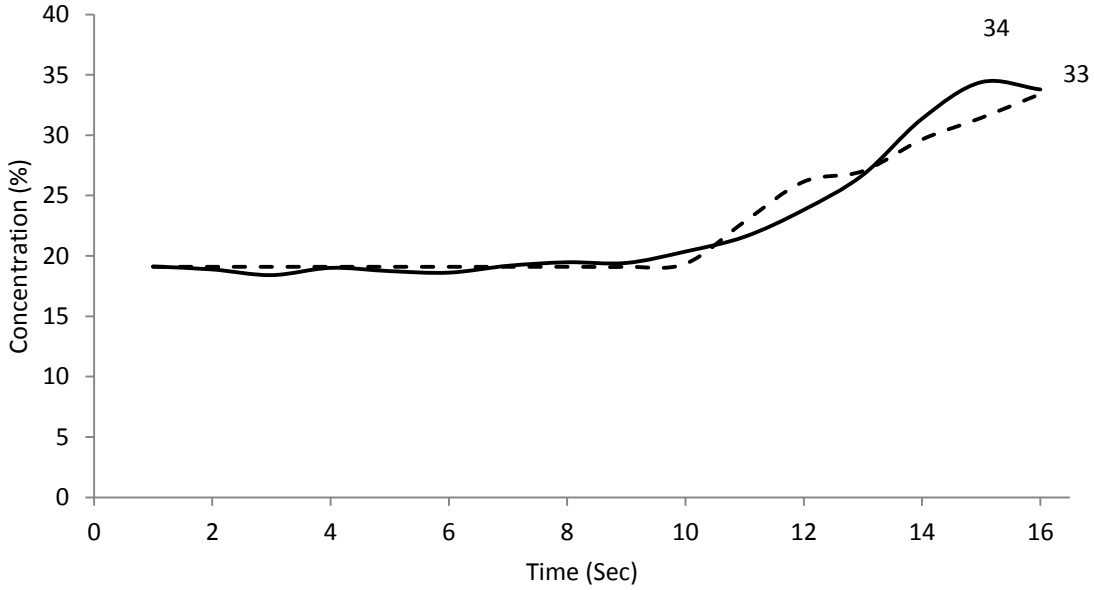

Time-concentration history plot for test 10 - Area 1

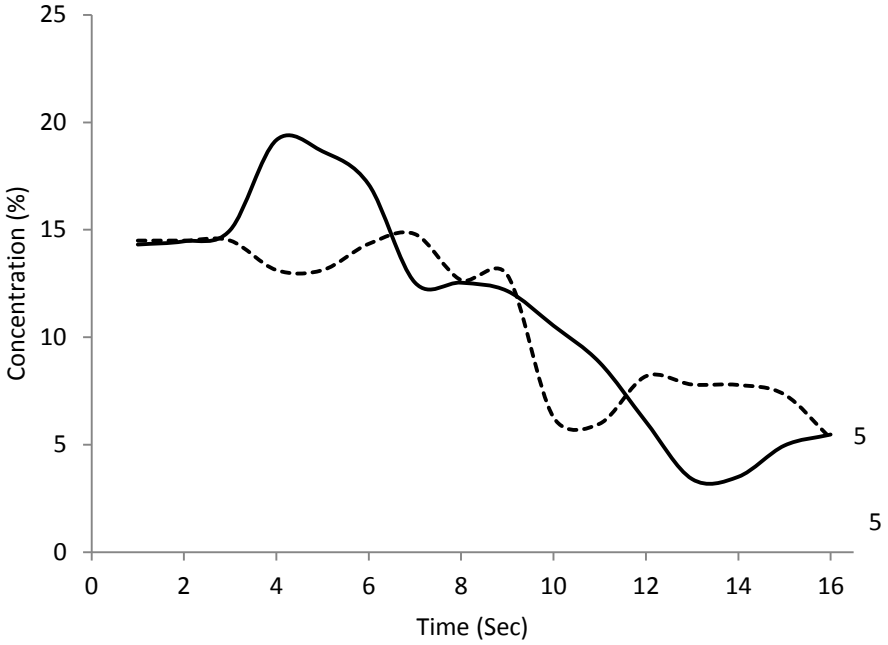

Time-concentration history plot for test 10 - Area 2

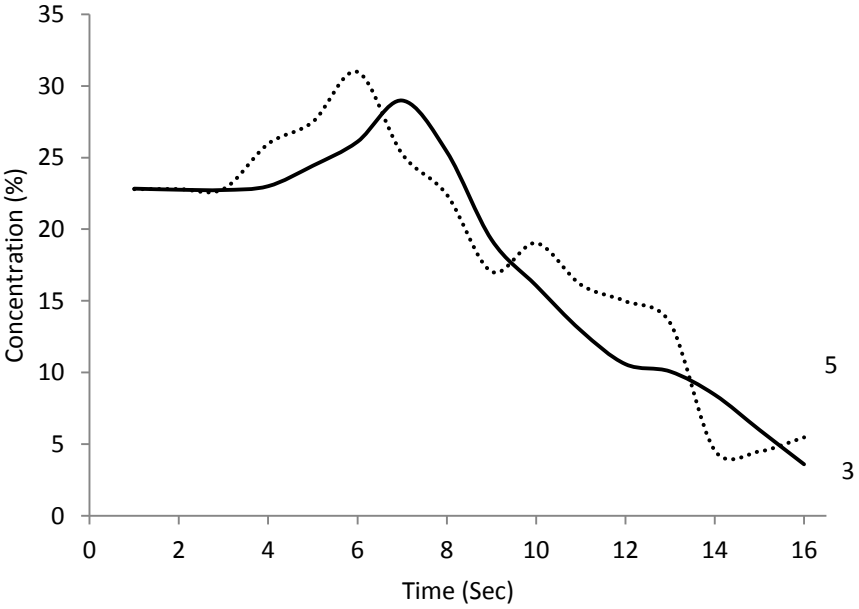

Time-concentration history plot for test 10- Area 3

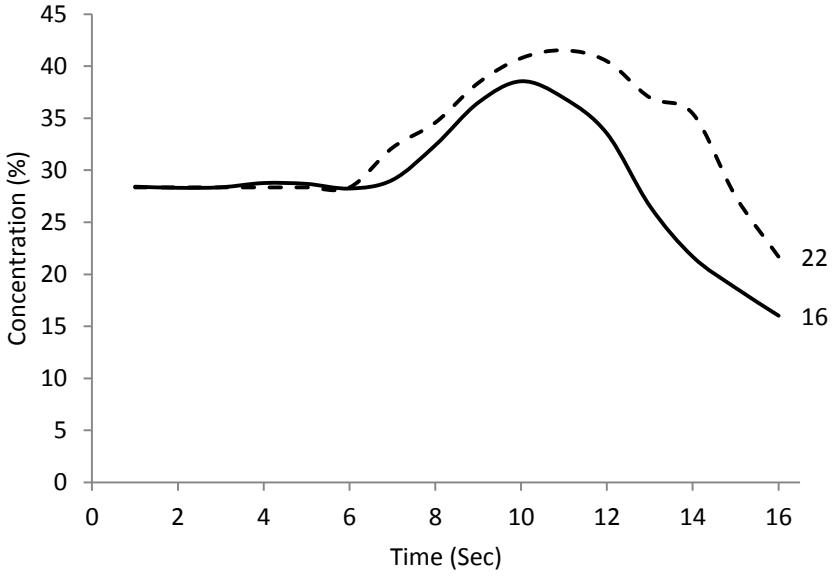

Time-concentration history plot for test 10 - Area 4

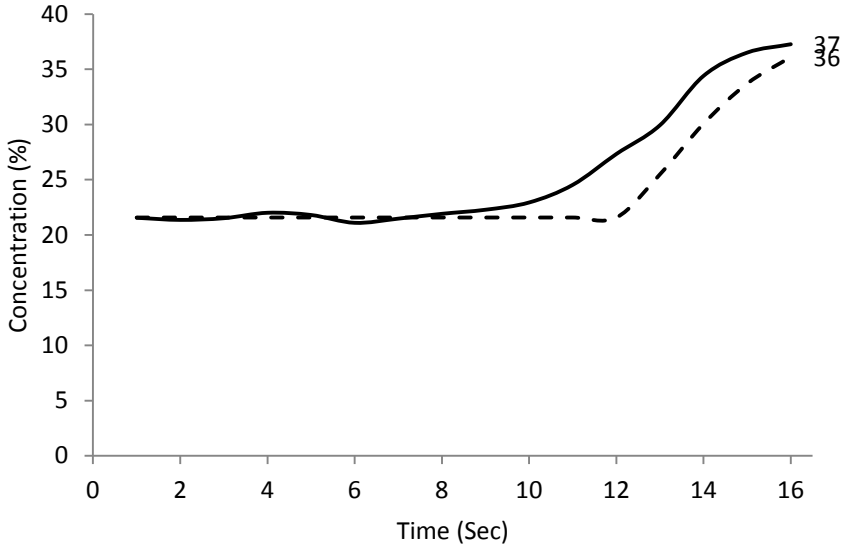

Time-concentration history plot for test 11 - Area 1

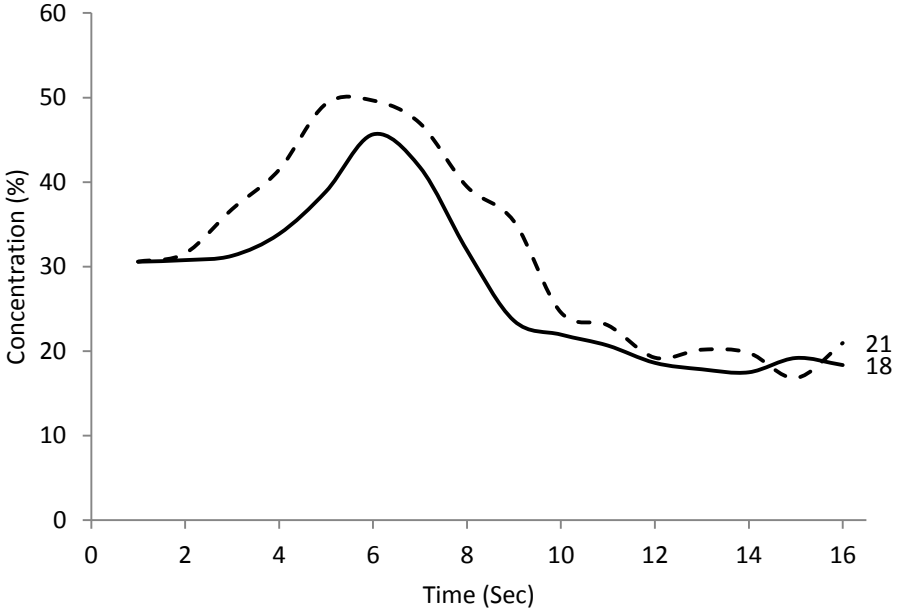

Time-concentration history plot for test 11 - Area 2

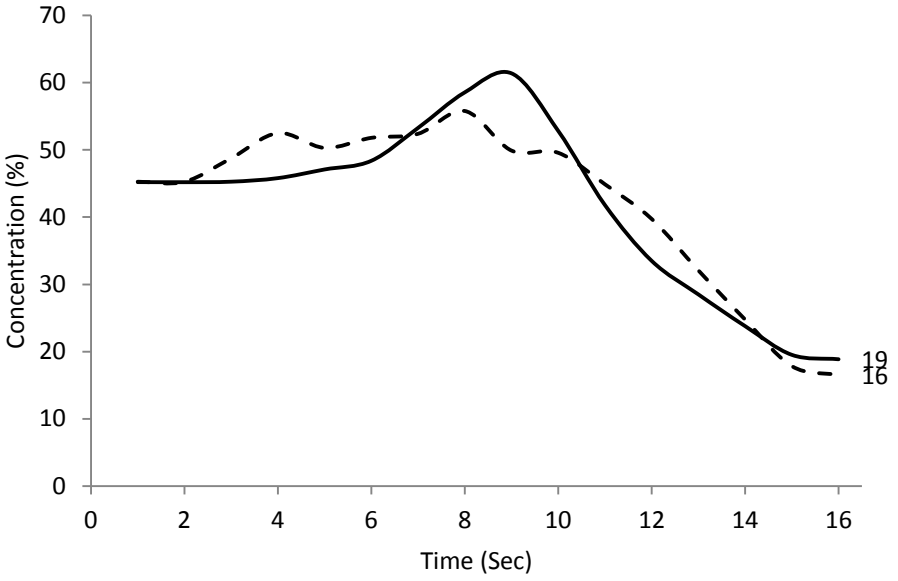

Time-concentration history plot for test 11- Area 3

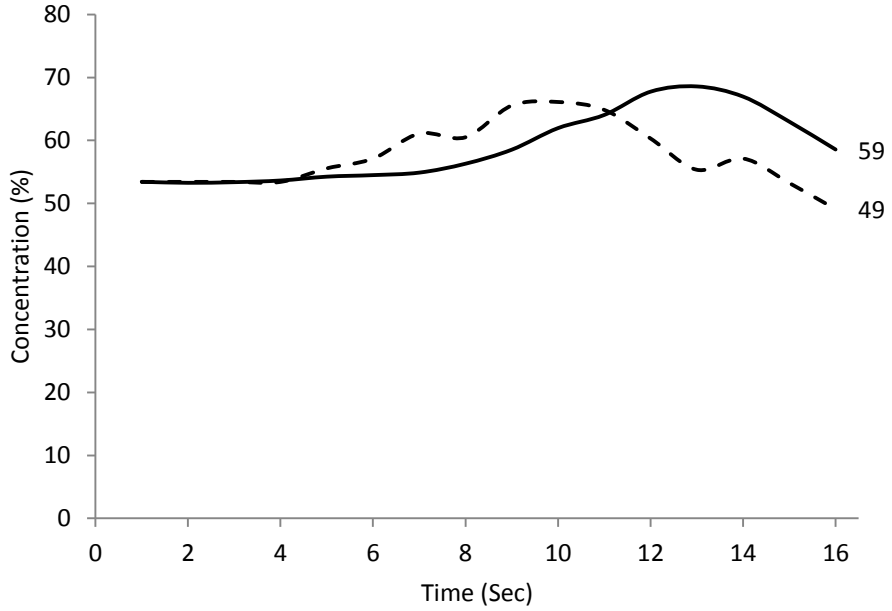

Time-concentration history plot for test 11 - Area 4

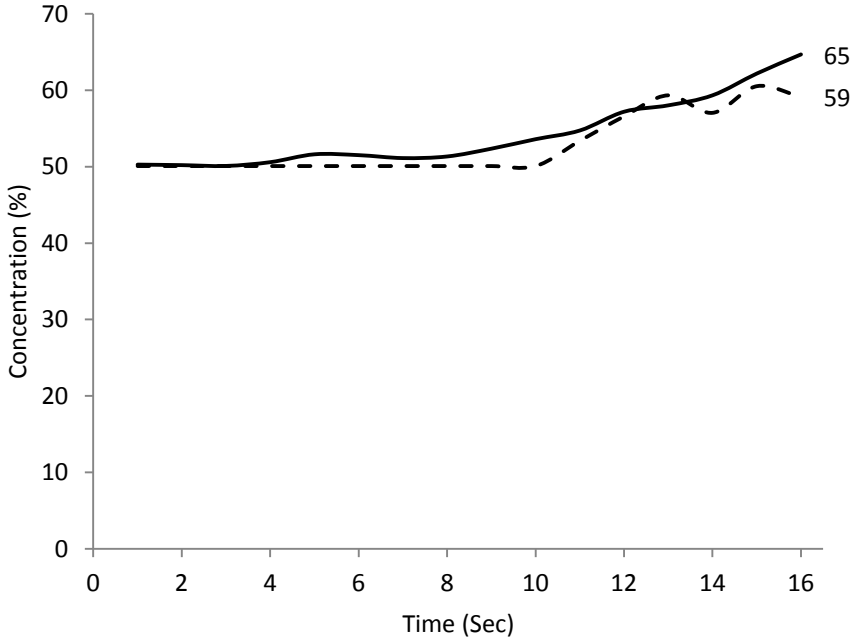

Time-concentration history plot for test 12 - Area 1

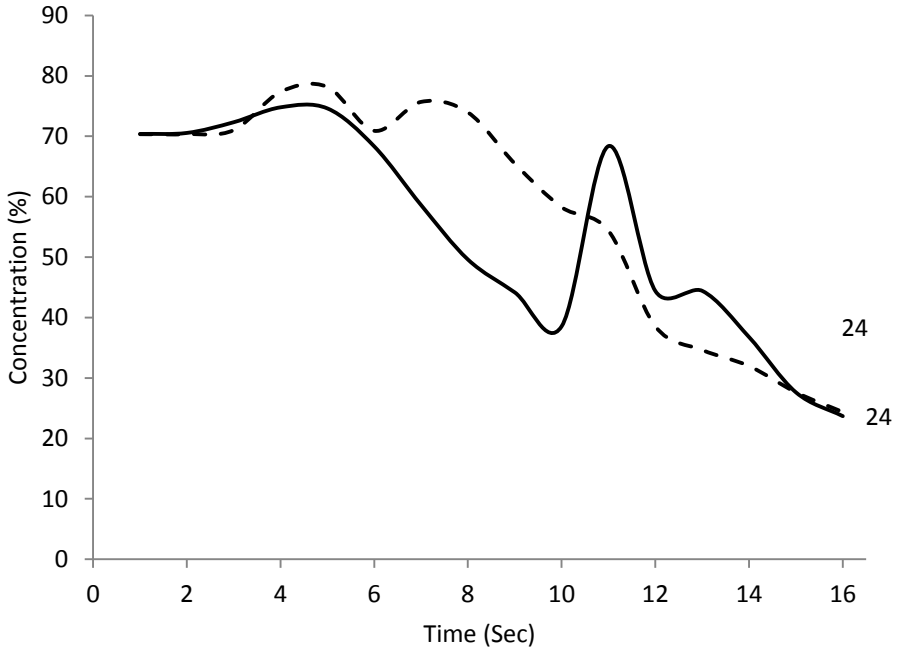

Time-concentration history plot for test 12 - Area 2

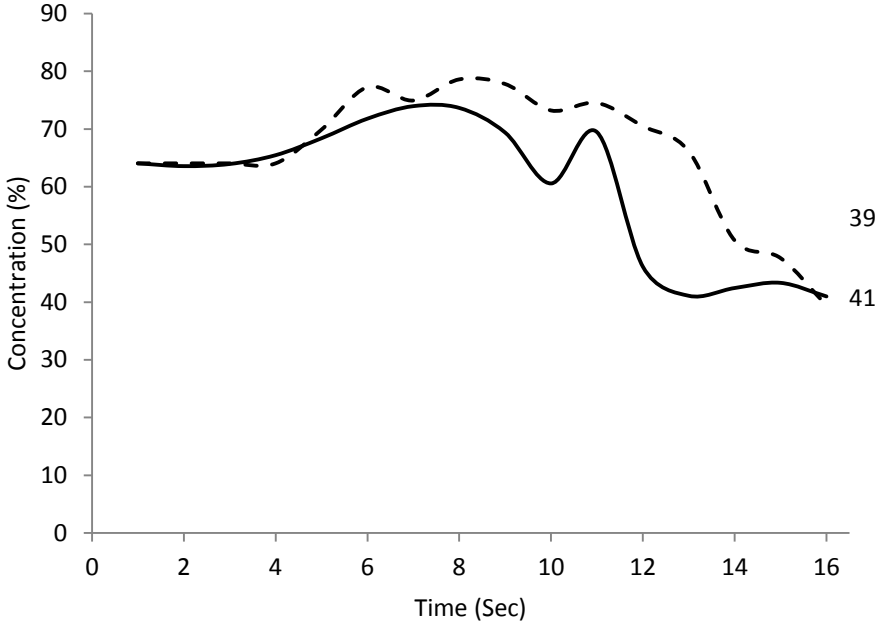

Time-concentration history plot for test 12- Area 3

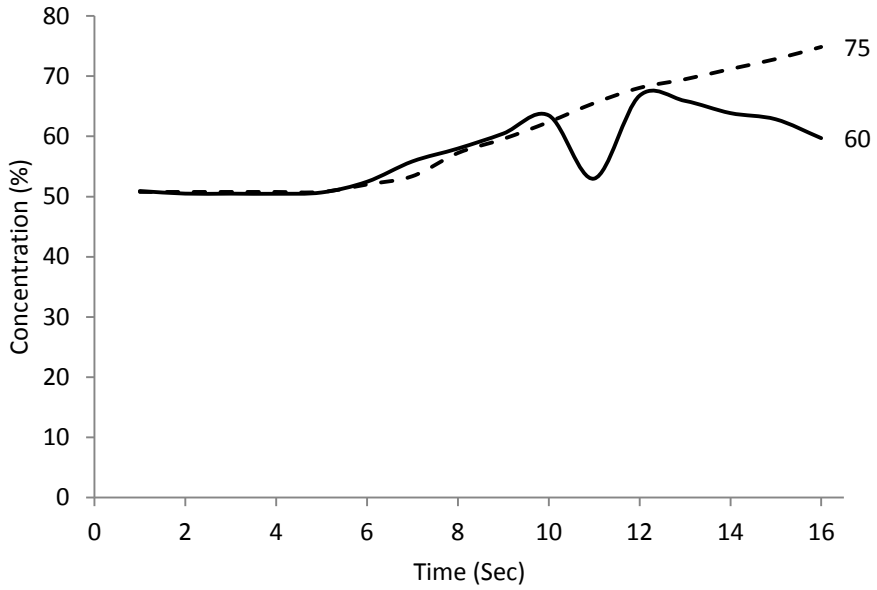

Time-concentration history plot for test 12 - Area 4

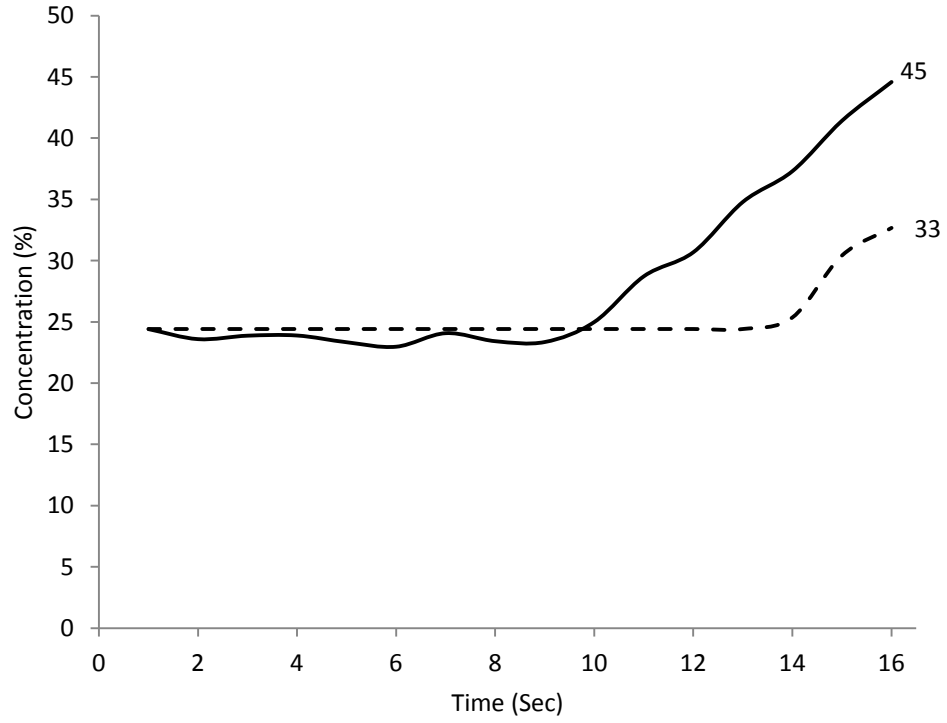

Appendix - B

Concentration in Areas 1, 2, 3 and 4 for 15 seconds at an interval of 1 second for both the experimental results and model predictions for Test 1-12.

Test -1 Result from Experiment

Time	Area 1	Area 2	Area 3	Area 4
0	22	28	34	30
1	22	28	34	30
2	22	28	34	30
3	25	28	34	30
4	29	29	34	30
5	22	35	34	30
6	21	35	35	30
7	16	33	39	30
8	14	27	44	30
9	11	21	45	31
10	8	17	44	32
11	6	15	42	36
12	5	11	34	39
13	4	9	28	43
14	3	6	22	46
15	2	6	17	48

Test -1 Results from Model

Time	Area 1	Area 2	Area 3	Area 4
0	22	28	34	30
1	22	28	34	30
2	26	28	34	30
3	29	29	34	30
4	30	30	35	30
5	29	30	37	30
6	26	28	40	30
7	21	29	43	30
8	16	30	44	30
9	15	27	45	31
10	15	23	39	38
11	12	20	35	41
12	12	17	31	43
13	12	13	28	46
14	12	10	27	45
15	11	8	25	46

Test - 2 Results from Experiment

Time	Area 1	Area 2	Area 3	Area 4
0	24	36	38	27
1	24	35	38	27
2	29	36	38	27
3	34	36	38	27
4	30	40	38	27
5	28	43	39	27
6	23	38	43	28
7	18	30	49	28
8	16	23	49	29
9	14	17	47	32
10	14	14	41	36
11	11	9	34	41
12	10	7	27	44
13	10	5	20	48
14	9	5	16	49
15	9	6	13	48

Test - 2 Results from Model

Time	Area 1	Area 2	Area 3	Area 4
0	24	36	38	28
1	24	36	38	28
2	25	36	38	28
3	25	36	38	28
4	26	38	38	28
5	24	41	39	28
6	23	36	43	28
7	20	33	46	28
8	17	29	49	28
9	12	26	50	28
10	12	22	51	28
11	12	20	48	28
12	12	17	44	32
13	9	10	40	35
14	7	10	37	33
15	7	10	29	37

Test -3 Results from Experiment

Time	Area 1	Area 2	Area 3	Area 4
0	66	59	44	41
1	67	60	43	41
2	69	60	43	40
3	72	64	44	40
4	68	68	46	40
5	54	71	48	40
6	47	70	53	40
7	40	63	58	40
8	32	54	62	41
9	29	43	66	43
10	26	37	61	48
11	23	35	54	53
12	19	30	47	58
13	18	24	41	63
14	18	20	34	66
15	18	18	30	65

Test -3 Results from Model

Time	Area 1	Area 2	Area 3	Area 4
0	66	59	44	41
1	66	59	44	41
2	70	59	44	41
3	64	70	44	41
4	58	73	45	41
5	53	75	50	41
6	48	74	53	41
7	39	69	58	41
8	33	65	64	41
9	32	53	68	42
10	28	47	65	47
11	23	36	64	50
12	22	28	60	52
13	21	25	52	52
14	20	21	45	57
15	20	23	38	58

Test - 4 Results from Experiment

Time	Area 1	Area 2	Area 3	Area 4
0	51	59	52	45
1	53	59	52	45
2	61	59	52	45
3	68	63	52	45
4	61	68	54	45
5	49	72	58	45
6	37	71	63	45
7	33	59	68	46
8	26	45	74	49
9	22	35	70	53
10	20	29	64	57
11	15	21	53	63
12	13	16	46	67
13	11	9	37	70
14	10	6	31	71
15	12	5	24	71

Test -4 Results from Model

Time	Area 1	Area 2	Area 3	Area 4
0	51	59	52	45
1	51	59	52	45
2	54	61	52	45
3	51	70	52	45
4	44	69	56	45
5	42	64	61	45
6	37	61	63	45
7	31	55	69	45
8	29	47	72	45
9	29	40	70	46
10	22	34	67	53
11	16	32	60	55
12	16	23	57	56
13	16	22	47	55
14	13	22	40	53
15	12	20	33	52

Test - 5 Results from Experiment

Time	Area 1	Area 2	Area 3	Area 4
0	49	45	40	38
1	48	44	40	37
2	48	44	40	37
3	48	44	40	37
4	50	44	40	37
5	54	44	40	37
6	57	45	40	37
7	58	47	40	38
8	56	49	40	38
9	52	53	40	37
10	47	56	41	38
11	44	58	41	38
12	42	58	42	37
13	39	57	44	37
14	37	56	45	37
15	37	54	47	38

Test - 5 Results from Model

Time	Area 1	Area 2	Area 3	Area 4
0	48	44	40	38
1	48	44	40	38
2	48	44	40	38
3	48	44	40	38
4	51	44	40	38
5	53	44	40	38
6	56	44	40	38
7	56	44	40	38
8	57	48	40	38
9	54	52	40	38
10	50	55	41	38
11	52	54	42	38
12	57	51	43	38
13	53	56	43	38
14	47	57	45	38
15	49	56	45	38

Test - 6 Results from Experiment

Time	Area 1	Area 2	Area 3	Area 4
0	22	25	36	31
1	22	25	35	30
2	23	25	35	30
3	26	25	35	30
4	28	26	36	30
5	23	30	36	30
6	19	33	36	30
7	19	32	36	30
8	18	27	40	30
9	16	23	43	31
10	14	21	44	32
11	13	21	42	32
12	12	20	40	34
13	12	18	37	36
14	13	17	34	39
15	13	15	32	41

Test - 6 Results from Model

Time	Area 1	Area 2	Area 3	Area 4
0	22	26	35	31
1	22	26	35	31
2	23	26	35	31
3	27	27	35	31
4	30	28	35	31
5	31	31	35	31
6	34	30	38	31
7	33	30	40	31
8	31	30	42	31
9	28	29	45	31
10	26	30	46	31
11	19	32	46	31
12	17	29	46	31
13	15	27	46	32
14	15	20	43	38
15	12	16	41	40

Test - 8 Results from Experiment

Time	Area 1	Area 2	Area 3	Area 4
0	26	29	37	34
1	26	29	36	33
2	26	29	37	33
3	26	29	36	33
4	29	29	37	34
5	36	29	37	33
6	34	30	37	33
7	30	34	38	34
8	27	36	37	32
9	27	34	40	33
10	27	28	43	33
11	22	27	48	33
12	22	22	52	33
13	19	20	50	36
14	18	19	43	38
15	18	18	38	43

Test - 8 Results from Model

Time	Area 1	Area 2	Area 3	Area 4
0	26	29	37	34
1	26	29	37	34
2	27	29	37	34
3	31	29	37	34
4	36	29	37	34
5	34	33	37	34
6	38	36	38	34
7	39	34	40	34
8	39	35	42	34
9	37	34	45	34
10	35	35	46	34
11	25	40	47	34
12	25	34	48	34
13	20	35	49	35
14	18	32	46	40
15	16	28	43	43

Test - 9 Results from Experiment

Time	Area 1	Area 2	Area 3	Area 4
0	18	26	13	19
1	18	26	13	19
2	19	26	13	18
3	22	27	13	19
4	24	27	13	19
5	21	32	14	19
6	18	36	15	19
7	17	33	19	19
8	17	21	26	19
9	17	15	29	20
10	13	15	27	22
11	9	13	23	24
12	7	10	20	27
13	5	8	13	31
14	5	6	8	34
15	3	4	5	34

Test - 9 Results from Model

Time	Area 1	Area 2	Area 3	Area 4
0	18	26	13	19
1	18	26	13	19
2	17	29	13	19
3	17	31	13	19
4	20	28	15	19
5	18	29	17	19
6	17	26	19	19
7	12	24	23	19
8	9	23	25	19
9	8	20	27	19
10	8	17	25	23
11	7	13	24	26
12	8	9	24	27
13	7	7	21	30
14	7	6	20	31
15	6	6	17	33

Test -10 Results from Experiment

Time	Area 1	Area 2	Area 3	Area 4
0	14	23	28	22
1	14	23	28	21
2	15	23	28	22
3	19	23	29	22
4	19	24	29	22
5	17	26	28	21
6	13	29	29	21
7	13	25	32	22
8	12	19	37	22
9	11	16	39	23
10	9	13	37	25
11	6	11	34	27
12	3	10	27	30
13	4	8	22	34
14	5	6	19	37
15	5	4	16	37

Test -10 Results from Model

Time	Area 1	Area 2	Area 3	Area 4
0	14	23	28	22
1	14	23	28	22
2	14	23	28	22
3	13	26	28	22
4	13	27	28	22
5	14	31	28	22
6	15	25	32	22
7	13	22	35	22
8	13	17	38	22
9	6	19	41	22
10	6	16	42	22
11	8	15	40	22
12	8	13	37	25
13	8	5	35	30
14	7	5	27	34
15	5	5	22	36

Test - 11 Results from Experiment

Time	Area 1	Area 2	Area 3	Area 4
0	31	45	53	50
1	31	45	53	50
2	31	45	53	50
3	34	46	54	51
4	39	47	54	52
5	46	48	55	51
6	42	53	55	51
7	32	59	56	51
8	24	61	59	52
9	22	53	62	54
10	21	42	64	55
11	19	33	68	57
12	18	29	69	58
13	17	24	67	59
14	19	20	63	62
15	18	19	59	65

Test - 11 Results from Model

Time	Area 1	Area 2	Area 3	Area 4
0	31	45	53	50
1	32	45	53	50
2	37	49	53	50
3	41	53	53	50
4	49	50	56	50
5	50	52	57	50
6	47	52	61	50
7	39	56	61	50
8	35	50	66	50
9	25	50	66	50
10	23	45	65	53
11	19	40	60	57
12	20	32	55	59
13	20	25	57	57
14	17	18	53	61
15	21	16	49	59

Test - 12 Results from Experiment

Time	Area 1	Area 2	Area 3	Area 4
0	70	64	51	24
1	71	64	50	24
2	72	64	50	24
3	75	65	50	24
4	75	68	51	23
5	68	72	52	23
6	59	74	56	24
7	50	74	58	23
8	44	69	60	23
9	39	61	63	25
10	68	69	53	29
11	44	46	67	31
12	44	41	66	35
13	37	42	64	37
14	28	43	63	41
15	24	41	60	45

Test - 12 Results from Model

Time	Area 1	Area 2	Area 3	Area 4
0	70	64	51	24
1	70	64	51	24
2	71	64	51	24
3	77	64	51	24
4	78	70	51	24
5	71	77	52	24
6	76	75	53	24
7	74	79	57	24
8	65	78	60	24
9	58	73	62	24
10	54	75	66	24
11	39	70	68	24
12	35	66	69	24
13	32	51	71	25
14	28	48	73	30
15	24	39	75	33

Appendix - C

C++ code developed for making model predictions

```
#include <iostream>
#include <conio.h>
#include <fstream>
#include <math.h>
#include <iomanip>
#include <string>
#include <time.h>
#include <windows.h>
#include <vector>

double n=12.5, Dp=0.2, Ct=0.17, U0, V0, W0, Rp=0.1, depth=0.2, DtoI=.4, angle=5,
inclineangle=angle*(3.14/180), CommonArea4=0, CommonArea3=0, CommonArea2=0,
CommonArea1=0;
float QX[20000][500], QY[20000][500], Xx[20000], Yy[20000], Ww[20000],
Areafinal1[20]={0,0,0,0,0,0,0,0,0,0,0,0,0,0,0,0,0,0,0,0},
Areafinal2[20]={0,0,0,0,0,0,0,0,0,0,0,0,0,0,0,0,0,0,0,0},
Areafinal3[20]={0,0,0,0,0,0,0,0,0,0,0,0,0,0,0,0,0,0,0,0},
Areafinal4[20]={0,0,0,0,0,0,0,0,0,0,0,0,0,0,0,0,0,0,0,0}, Check1x[20000][20],
Check1y[20000][20], Check1d[20000][20], Check2x[20000][20], Check2y[20000][20],
Check2d[20000][20], Check3x[20000][20], Check3y[20000][20], Check3d[20000][20],
Check4x[20000][20], Check4y[20000][20], Check4d[20000][20];
int Noofpiece=365, Areacountfinal1[20]={0,0,0,0,0,0,0,0,0,0,0,0,0,0,0,0,0,0,0,0},
Areacountfinal2[20]={0,0,0,0,0,0,0,0,0,0,0,0,0,0,0,0,0,0,0,0},
Areacountfinal3[20]={0,0,0,0,0,0,0,0,0,0,0,0,0,0,0,0,0,0,0,0},
Areacountfinal4[20]={0,0,0,0,0,0,0,0,0,0,0,0,0,0,0,0,0,0,0,0},  Checkcount1=0,
Checkcount2=0, Checkcount3=0, Checkcount4=0, TimeCount;

using namespace std;

float axialcomponentvalueplume (double x, double y)
{
double Umaxvalue,Umaxycor,angle,b1,R,b,Uvalue,Udelta,Udeltamax ;
Umaxycor= 0.53*Dp/2;
R= Umaxycor;
b=Dp/2+.15*x;
b1=y;
if( x/Dp < 3.25 )
{
Umaxvalue= U0*(1 - .1592*(x/Dp));
Uvalue = abs((Umaxvalue));
}
else
if ( x/Dp <= 16 )
{
```

```
Umaxvalue=0.638*U0*exp(-0.097*(x/Dp));
Uvalue = Umaxvalue;
}
else
if (x/Dp > 16 )
{
Umaxvalue = .638*exp(-1.552)*U0*exp(-0.69*pow(((x-16*Dp)),2)/pow(25*Dp,2));
Uvalue = Umaxvalue;
}
return Uvalue;
}

float axialcomponentvalue (double x, double y)
{
double Umaxvalue,Umaxycor,angle,b1,R,b,Uvalue,Udelta,Udeltamax,xtouch,xcentre ;
Umaxycor= 0.53*Dp/2;
R= Umaxycor;
xtouch = (depth-Dp/2)/tan(8.5*(3.14/180)+inclineangle);
xcentre = (depth-Dp/2)/tan(inclineangle);
if ( Dp/2+.15*x+x*tan(inclineangle) < depth )
b=(Dp/2+.15*x);
else
b=(Dp/2+.32*x);
if (inclineangle>0)
{
if(x<xcentre)
b1=sqrt(pow((depth-x*tan(inclineangle)),2)+pow(y,2));
else
b1=y;
}
else
b1=sqrt(pow(depth,2)+pow(y,2));
if( x/Dp < 3.25 )
{
Umaxvalue= U0*(1 - .1592*(x/Dp));
if( x < xcentre )
Uvalue = abs((Umaxvalue*exp(-0.69*pow((b1-R),2)/pow(b,2)))*cos(inclineangle));
else
Uvalue = abs((Umaxvalue*exp(-0.69*pow((b1-R),2)/pow(b,2))));
}
else
if ( x/Dp <= 16 )
{
Umaxvalue=0.638*U0*exp(-0.097*(x/Dp));
```

```
if( x < xcentre )
Uvalue = Umaxvalue*exp(-0.69*pow((b1),2)/pow(b,2))*cos(inclineangle);
else
Uvalue = Umaxvalue*exp(-0.69*pow((b1),2)/pow(b,2));
}
else
if (x/Dp > 16 )
{
Umaxvalue = .638*exp(-1.552)*U0*exp(-0.69*pow(((x-16*Dp)),2)/pow(25*Dp,2));

if( x < xcentre )
Uvalue = Umaxvalue*exp(-0.69*pow((b1),2)/pow(b,2))*cos(inclineangle);
else
Uvalue = Umaxvalue*exp(-0.69*pow((b1),2)/pow(b,2));
}
return Uvalue;
}

double tangentialcomponentvalue (double x, double y)
{
double Vmaxvalue,Vmaxycor,angle,b1,R,b,Vvalue,Vdelta,Vdeltamax ;
V0=0.82*U0;
b1=sqrt(pow(depth,2)+pow(y,2));
b=(Dp/2+.32*x);
Vvalue=0;
if( x/Dp < 0.79)
{
Vmaxvalue=(-0.6952*(x/Dp)+0.9743)*V0;
Vmaxycor=0.13+(x/Dp)*(.53-.13)/1.05;
R=Vmaxycor;
Vvalue =Vmaxvalue*exp(-pow((b1-R),2)/pow(b,2));
}
else
if( x/Dp < 6.2)
{
Vmaxvalue=V0*(0.7031*exp(-0.4998*(x/Dp)));
if( x/Dp < 1.05 )
Vmaxycor=0.13+(x/Dp)*(.53-.13)/1.05;
else
if( x/Dp < 2.1 )
Vmaxycor=0.53+(x/Dp)*(.13-.53)/(2.1-1.05);
else
if( x/Dp < 4.74 )
```

```
Vmaxycor=0.13+(x/Dp)*(1.58-.13)/(4.74-2.1);
else
if( x/Dp < 5.2 )
Vmaxycor=1.58+(x/Dp)*(0.78-1.58)/(5.2-4.74);
else
if( x/Dp < 6.05 )
Vmaxycor=.78+(x/Dp)*(1.84-.78)/(6.05-5.2);
                                                    else
if( x/Dp <= 6.2 )
Vmaxycor=1.84+(x/Dp)*(1.3-1.84)/(6.32-6.05);
R = 0;
Vvalue =Vmaxvalue*exp(-pow((b1-R),2)/pow(b,2));
}
else
if(  x/Dp < 50 && y < 0.25*b && y > -0.25f*b )
{
Vmaxvalue=0;
R=0;
Vvalue =Vmaxvalue;
}
else
if(  x/Dp < 50 && y < 1.5*b && y > -1.5f*b )
{
Vmaxvalue=0.05*V0;
R=0;
Vvalue =Vmaxvalue;
}
return Vvalue;
}

void forcefield (double x, double y, double d, int j )
{
float
Vt[20000],V[20000],dis[20000],a[20000],Rho=1000.00,h=.0127,d1=d,m=3.14*Rho*h*p
ow((d1/2),2);
float Vty[20000],Vy[20000],disy[20000],ay[20000];
float Vtplume[20000], displume[20000];
int i,k=0,hi=0,TimeforResults=0;
float Fwd,Fp;
float Fwdy,Fpy;

dis[0]= x+DtoI;
disy[0]= y;
displume[0] =0 ;
```

```
V[0]=0;
Vy[0]=0;
Vt[0]= axialcomponentvalue( dis[0],disy[0]);
Vty[0]= tangentialcomponentvalue(dis[0],disy[0]);
Vtplume[0] = axialcomponentvalueplume ( displume[0],0);

ofstream output("output.txt",ios::out | ios::app);
output<<"i     "<<"j        "<<"dis[i]       "<<endl;
ofstream test4area("test4area.txt",ios::out | ios::app);

double r1,r2,x1,x2,x3,x4,y1,y2,a1,a2,Area1=0,Area2=0;

for (i=1;i<2500;i++)
{
Vtplume[i] = axialcomponentvalueplume ( displume[i-1],0);
displume[i]=displume[i-1] + Vtplume[i]*0.01;
if ( dis[i-1]< displume[i]+2)
{
Vt[i]= axialcomponentvalue( dis[i-1],disy[i-1]);
Fp=0.5*Rho*d*h*((Vt[i]-Vt[i-1])/0.01);
Fwd=0.5*Rho*d*h*pow(V[i-1]-Vt[i],2);
a[i]=  ((Vt[i]-Vt[i-1])/0.01)  + (Fwd)/m;
V[i]=V[i-1]+a[i]*(.01);
dis[i]=dis[i-1] + V[i]*(.01);
if ( dis[i-1]< displume[i])
{
Vty[i]= tangentialcomponentvalue( dis[i-1],disy[i-1]);
Fpy=0.5*Rho*d*h*((Vty[i]-Vty[i-1])/0.01);
Fwdy=0.5*Rho*d*h*pow(Vy[i-1]-Vty[i],2);
ay[i]=((Vty[i]-Vty[i-1])/0.01)+(Fwdy)/m;
if (disy[i-1] >= 0
{
Vy[i]=Vy[i-1]+ay[i]*(.01);
if (disy[i-1]>=2)
{
disy[i]=2;
}
else
disy[i]=disy[i-1]+ Vy[i]*(.01);
}
else
{
Vy[i]=Vy[i-1]+ay[i]*(.01);
if (disy[i-1]<=-2)
```

```
{
disy[i]=-2;
}
else
disy[i]=disy[i-1]- Vy[i]*(.01);
}
}
else
{
disy[i]=disy[i-1];
Vty[i]= tangentialcomponentvalue( dis[i-1],disy[i-1]);
Vy[i]=0;
}
}
else
{
dis[i]=dis[i-1];
disy[i]=disy[i-1];
Vt[i]= axialcomponentvalue( dis[i-1],disy[i-1]);
Vty[i]= tangentialcomponentvalue( dis[i-1],disy[i-1]);
V[i]=0;
Vy[i]=0;
}
{ QX[k ][j]= dis[i]-DtoI; QY[k ][j]= disy[i]; k++;}
}
cout <<"Ice Floe ";  cout<<j<<endl;
output<<"     "<<endl;
}

float area(float X[], float Y[], float D[], double Up, double Low)
{
int i,j,count=0,hi;
float r1, r2, x1, x2, y1, y2, Xt[1000], Yt[1000], Dt[1000], a1, a2, Area=0, Area1=0,
Area2=0, Area4=0, x3, x4, Aread=0;

for (i=0; i<Noofpiece; i++)
{
if  (X[i]<Up && X[i]>=Low )
{
count++;
Xt[count]=X[i];
Yt[count]=Y[i];
Dt[count]=D[i];
x1=X[i];
```

```
y1=Y[i];
r1=D[i]/2;

for( hi=1;hi<count;hi++)
{
x2=Xt[hi];
y2=Yt[hi];
r2=Dt[hi]/2;
Area1=0;
Area2=0;
if (sqrt(pow((x1-x2),2)+pow((y1-y2),2))<abs(r1-r2))
{
if (r1<r2)
{Area1 =0; //3.14*pow(r1,2);
Area2=0;
}
else
{Area1 = 0;// 3.14*pow(r2,2);
Area2=0;
}
}
else
if (sqrt(pow((x1-x2),2)+pow((y1-y2),2))<(r1+r2))
{
x3=r1*(sqrt(pow((x1-x2),2)+pow((y1-y2),2))/(r1+r2));
x4=r2*(sqrt(pow((x1-x2),2)+pow((y1-y2),2))/(r1+r2));
a1=acos(x3/r1);a2=acos(x4/r2);
Area1=pow(r1,2)*(a1-sin(a1)*cos(a1));
Area2=pow(r2,2)*(a2-sin(a2)*cos(a2));
}
Aread=Aread+Area1+Area2;
}
Area4= Area4 + 3.14*pow(r1,2);
}
}
Area= Area4 -Aread;
cout<<"DArea :"<<Area<<" Total area : "<<Area4<<endl;
return Area;
}

void main()
{
double Umaxvalue,Umaxycor, Vmaxvalue,Vmaxycor, Wmaxvalue,Wmaxycor;
double x,y,Area1=0,Area2=0,Area3=0,Area4=0;
```

```
float Xtransfer[1000],Ytransfer[1000];
U0=1.59*n*Dp*pow(Ct,0.5);
int i,j,Areacount1=0,Areacount2=0,Areacount3=0,Areacount4=0,kk=1;

ifstream X ("X.txt");
ifstream Y ("Y.txt");
ifstream W ("W.txt");
for (i=0; i<Noofpiece; i++ ) //1000   Changes made for one piece
{
if (X.is_open())
{
X>>Xx[i];
Y>>Yy[i];
W>>Ww[i];
forcefield(Xx[i],Yy[i],Ww[i],i);
}
}

for (j=1;j<1502;j=j+100)
{
for (i=0;i<Noofpiece;i++)
{
Xtransfer[i]=QX[j][i];
Ytransfer[i]=QY[j][i];
}
Areafinal1[kk]=area(Xtransfer, Ytransfer, Ww, 2.8, 2);
Areafinal2[kk]=area(Xtransfer, Ytransfer, Ww, 3.6, 2.8);
Areafinal3[kk]=area(Xtransfer, Ytransfer, Ww, 5, 3.6);
Areafinal4[kk]=area(Xtransfer, Ytransfer, Ww, 6.5, 5);
kk++;
}
output.close();
outputy.close();

cout<<endl<<endl<<" Total Area = 2.6"<<endl;

for (i=0; i<Noofpiece; i++)
{
if  (Xx[i]>=5 && Xx[i]<6.5 )
{
Areacount4++;
Area4 = Area4 + 3.14*pow(Ww[i],2)/4;
}
if  (Xx[i]>=3.6 && Xx[i]<5 )
```

```
{
Areacount3++;
Area3 = Area3 + 3.14*pow(Ww[i],2)/4;
}
if  (Xx[i]>=2.8 && Xx[i]<3.6 )
{
Areacount2++;
Area2 = Area2 + 3.14*pow(Ww[i],2)/4;
}
if  (Xx[i]>=2 && Xx[i]<2.8  )
{
Areacount1++;
Area1 = Area1 + 3.14*pow(Ww[i],2)/4;
}
}
ofstream Results ("Results.csv", ios::out | ios::trunc);
cout<<endl<<"200"<<","<<100*Area1/(4*0.8)<<","<<100*Area2/(4*0.8)<<","<<100*A
rea3/(4*1.4)<<","<<100*Area4/6<<","<<endl;
Results <<endl<<"Time,"<<"Yellow,"<<"Green,"<<"Blue,"<<"Red,"<<endl;
for(i=0;i<16;i++)
{
Results<<i+1<<","<<100*(Areafinal1[i+1])/(4*.8)<<","<<100*(Areafinal2[i+1])/(4*.8)<
<","<<100*(Areafinal3[i+1])/(1.4*4)<<","<<100*(Areafinal4[i+1])/6<<","<<endl;
}
Results <<endl<<"After Deduction,"<<endl;
Results <<"Time,"<<"Yellow,"<<"Green,"<<"Blue,"<<"Red,"<<endl;
for(i=0;i<16;i++)
{
Results<<i+1<<","<<100*(Area1-Areafinal1[i+1])/(4*0.8)<<","<<100*(Area2-
Areafinal2[i+1])/(4*0.8)<<","<<100*(Area3-reafinal3[i+1])/(4*1.4)<<","<<100*(Area4-
Areafinal4[i+1])/6<<","<<endl;
}
cout<<endl<<"End";
getch();
}
```

Appendix- D

MATLAB code used for Image Analysis of Images extracted from experimental videos.

```
Basename = 'C:\Users\Tony\Dropbox\Thesis Support Documents Sorted\Jennas
Comparison\Softwares and codes\Images Pure\';
Lastname = '.jpg';

for k=3
Sheetname=['Run - ',num2str(k)];
Header = {'Time', 'Yellow ', 'Green','Blue','Red'}
xlswrite('C:\Users\Tony\Dropbox\Thesis Support Documents Sorted\Jennas
Comparison\Softwares and codes\Images Pure\Percent of White
Pixels.xlsx',Header,Sheetname)

for h = 1:16
Filename=[Basename,num2str(k),'\',num2str(h),Lastname];
Filename1=[Basename,num2str(k)];
mkdir(Filename1,'Image Processed')
Filename2=[Basename,num2str(k),'\Image Processed\',num2str(h),Lastname];

f=figure();
grayImage=imread(Filename);
[Rows Colums Numberofcolorbands]=size(grayImage);
subplot(2,2,1);
imshow(grayImage);
title('Original Grayscale Image','FontSize',20);
set(gcf,'Position',get(0,'Screensize'));
grayImage=rgb2gray(grayImage);
[pixelCount grayLevels]=imhist(grayImage)
subplot(2,2,2);
bar(pixelCount);
title('Histogram of Original Image','FontSize',20);
xlim([0 grayLevels(end)]);
binaryImage=grayImage>230
subplot(2,2,3);
imshow(binaryImage);
title('Binary Image','FontSize',20);
hold on

numberOfBlackPixelsinYellow = 0;
numberOfWhitePixelsinYellow = 0;
for i=695:855
a = int16(-.1875*i+165.3125)
b = int16(0.2875*i+801.1875)
for j= a:b
if binaryImage(i,j) == 0
numberOfBlackPixelsinYellow=numberOfBlackPixelsinYellow+1;
```

```
else
numberOfWhitePixelsinYellow=numberOfWhitePixelsinYellow+1;
end
end
end

totalNumberOfPixelsinYellow =
numberOfBlackPixelsinYellow+numberOfWhitePixelsinYellow;
percentBlackPixelsinYellow=100.0*numberOfBlackPixelsinYellow/totalNumberOfPixel
sinYellow;
percentWhitePixelsinYellow=100.0*numberOfWhitePixelsinYellow/totalNumberOfPixel
sinYellow;

numberOfBlackPixelsinGreen = 0;
numberOfWhitePixelsinGreen = 0;
for i=535:695
a = int16(-.4625*i+356.44)
b = int16(0.29375*i+796.84)
for j= a:b
if binaryImage(i,j) == 0
numberOfBlackPixelsinGreen=numberOfBlackPixelsinGreen+1;
else
numberOfWhitePixelsinGreen=numberOfWhitePixelsinGreen+1;
end
end
end

totalNumberOfPixelsinGreen =
numberOfBlackPixelsinGreen+numberOfWhitePixelsinGreen;
percentBlackPixelsinGreen=100.0*numberOfBlackPixelsinGreen/totalNumberOfPixelsin
Green;
percentWhitePixelsinGreen=100.0*numberOfWhitePixelsinGreen/totalNumberOfPixelsi
nGreen;

numberOfBlackPixelsinBlue = 0;
numberOfWhitePixelsinBlue = 0;
for i=375:535
a = int16(-.46875*i+359.7812)
b = int16(0.2875*i+800.1875)
for j= a:b
if binaryImage(i,j) == 0
numberOfBlackPixelsinBlue=numberOfBlackPixelsinBlue+1;
else
numberOfWhitePixelsinBlue=numberOfWhitePixelsinBlue+1;
```

```
end
end
end

totalNumberOfPixelsinBlue =
numberOfBlackPixelsinBlue+numberOfWhitePixelsinBlue;
percentBlackPixelsinBlue=100.0*numberOfBlackPixelsinBlue/totalNumberOfPixelsinBl
ue;
percentWhitePixelsinBlue=100.0*numberOfWhitePixelsinBlue/totalNumberOfPixelsinBl
ue;

numberOfBlackPixelsinRed = 0;
numberOfWhitePixelsinRed = 0;
for i=215:375
a = int16(-.4625*i+357.4375)
b = int16(0.292375*i+797.84375)
for j= a:b
if binaryImage(i,j) == 0
numberOfBlackPixelsinRed=numberOfBlackPixelsinRed+1;
else
numberOfWhitePixelsinRed=numberOfWhitePixelsinRed+1;
end
end
end

totalNumberOfPixelsinRed = numberOfBlackPixelsinRed+numberOfWhitePixelsinRed;
percentBlackPixelsinRed=100.0*numberOfBlackPixelsinRed/totalNumberOfPixelsinRed
;
percentWhitePixelsinRed=100.0*numberOfWhitePixelsinRed/totalNumberOfPixelsinRe
d;

p1=[535,954];
p2=[375,908];
plot([p1(2),p2(2)],[p1(1),p2(1)],'Color','b','LineWidth',2);
p1=[375,184];
p2=[535,109];
plot([p1(2),p2(2)],[p1(1),p2(1)],'Color','b','LineWidth',2);

p1=[535,954];
p2=[695,1001];
plot([p1(2),p2(2)],[p1(1),p2(1)],'Color','g','LineWidth',2);
p1=[695,35];
p2=[535,109];
plot([p1(2),p2(2)],[p1(1),p2(1)],'Color','g','LineWidth',2);
```

```
p1=[215,861];
p2=[375,908];
plot([p1(2),p2(2)],[p1(1),p2(1)],'Color','r','LineWidth',2);
p1=[375,184];
p2=[215,258];
plot([p1(2),p2(2)],[p1(1),p2(1)],'Color','r','LineWidth',2);


p1=[855,1047];
p2=[695,1001];
plot([p1(2),p2(2)],[p1(1),p2(1)],'Color','y','LineWidth',2);
p1=[695,35];
p2=[855,0];
plot([p1(2),p2(2)],[p1(1),p2(1)],'Color','y','LineWidth',2);
hold off

PlaceinSheet =['A',num2str(h+1)];
Header = {h,
percentWhitePixelsinYellow,percentWhitePixelsinGreen,percentWhitePixelsinBlue,perce
ntWhitePixelsinRed}
xlswrite('C:\Users\Tony\Dropbox\Thesis Support Documents Sorted\Jennas
Comparison\Softwares and codes\Images Pure\Percent of White
Pixels.xlsx',Header,Sheetname,PlaceinSheet)

saveas(f,Filename2)
hold off;
close (f);
end
end
```

Appendix - E

Co-ordinates used to define Areas 1, 2, 3, and 4 for Test 1 to Test 12.

[(1047, 855), (5, 855), (1001, 695), (35, 695)]

[(1001, 695), (35, 695), (954, 535), (109, 535)]

[(954, 535), (109, 535), (908,375), (184,375)]

[(908,375), (184,375), (861, 215), (258, 215)]